Report No. TE 23-66

Thermo Electron Engineering Corporation, 85 First Avenue, Waltham, Massachusetts 02154

This work was performed for the Jet Propulsion Laboratory, California Institute of Technology, sponsored by the National Aeronautics and Space Administration under Contract NAS7-100.

FIRST QUARTERLY PROGRESS REPORT

APPLIED THERMIONIC RESEARCH

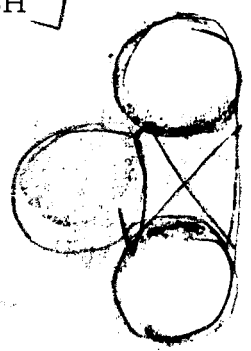

Contract 951262

25 June to 25 September 1965

by

S. Kitrilakis
D. Lieb
F. Rufeh
L. van Someren

Prepared for

Jet Propulsion Laboratory
Pasadena, California

Approved by S. Kitrilakis

S. Kitrilakis
Research Manager

TABLE OF CONTENTS

TABLE OF CONTENTS (continued)

LIST OF ILLUSTRATIONS

LIST OF ILLUSTRATIONS (continued)

CHAPTER I

INTRODUCTION AND SUMMARY

The primary objective of this program is the study of two types of Cs-vapor thermionic converters. The first type uses cesium fluoride vapor in addition to metallic cesium. The use of cesium fluoride provides one additional degree of freedom in obtaining given electrode work functions. The second type of converter uses an inert gas in addition to cesium. It is expected that, under proper conditions, the presence of the inert gas will aid in the conservation of ions generated in the inter-electrode volume and thus reduce the internal voltage drop. The experimental study of both schemes of thermionic conversion is divided into two classes of experiments. The first class of experiments is more basic in nature and consists primarily of determining the effect of the CsF and inert-gas additives on electrode work functions for the former, and on the plasma for the latter. The second class of experiment is the generation of parametric-type performance data over wide ranges of variation of converter parameters. The basic experiments precede the parametric studies, since it is expected that they will guide the selection of conditions which will optimize the effects of these additives. In parallel with the experimental programs outlined above, analytical and correlation work will be conducted, its objective being the formulation of valid physical models and the quantitative description of the processes.

The cesium fluoride additive work is a direct continuation of the program of the previous year under JPL Contract No. 950671/NAS7-100. The program demonstrated very impressive performance with CsF, which, however, could not be maintained over long periods of time. A specific

objective of the present work is to obtain the enhanced performance in a stable manner and then define it parametrically over a wide range.

The inert gas "plasma additive" concept is an outgrowth of the analytical work done in the previous year under the contract named above.

The equipment and test converter were, of course, available from the same contract. A great deal of effort was expended in that program on the test converter, and the result was a very versatile, accurate and reliable device.[19] A few modifications had to be made, mainly to admit the inert gas and to allow the use of a larger bell jar. These are described in Chapter II.

The preparation and examinations performed to date on the emitter surfaces are given in Chapter IV. These techniques were also developed during the previous year.

Argon was selected for the first experiments with inert-gas additives. The reasons for the selection of this gas, as well as the model postulated to explain the effects of the gas, are discussed in Chapter III.

The fabrication of devices and auxiliaries is now essentially completed. The experimental program is in its initial phases, and the work completed to date is concerned mainly with the measurement of surface work functions in vacuum for both Re and W surfaces, and in the presence of CsF for the W emitter. Although this phase is by no means completed, the variation of the W work function in the CsF pressure is much more consistent and reproducible than in previous experiments. In fact, as shown in Chapter V, even at this time meaningful correlation appears possible.

The data obtained with the rhenium emitter to date are shown in Chapter VI.

CHAPTER II

TEST CONVERTER AND EQUIPMENT

The test converters used in this program are variable parameter research-type devices. They are of planar geometry and use an active collector guard ring. The parameters whose values can be varied and accurately controlled include the emitter temperature, the interelectrode spacing, the collector and reservoir temperatures, and, of course, the output. The active collector guard ring is a very desirable feature since it renders the conversion process free of any radial geometric dependence. The elimination of edge effects is possible because the voltage and temperature of the guard ring can be adjusted to be equal to those of the collector at all times. The gap between collector and guard ring, shown in Figure II-1, is kept to a value close to 1 mil. The height of the step between the collector and guard ring is kept at approximately 1/2 mil, with the collector protruding beyond the guard-ring surface.

The emitter is heated by electron bombardment, and its temperature is measured with an optical pyrometer in a black-body cavity located on its back surface. The collector and guard-ring temperatures are maintained by balancing the heat input to their respective heaters against the heat rejected to individual water-cooled coils. The variation of spacing is accomplished by flexing a bellows joining the emitter and collector structures by means of a mechanism operated externally to the bell jar. Figure II-2 shows how this is accomplished. Three micrometer spindles (part No. 61) are driven by shafts (98) which are geared together above the top plate. The interelectrode spacing is measured directly on three dial indicators (part No. 1) which are

Figure II-1

Cross Section of Test Converter

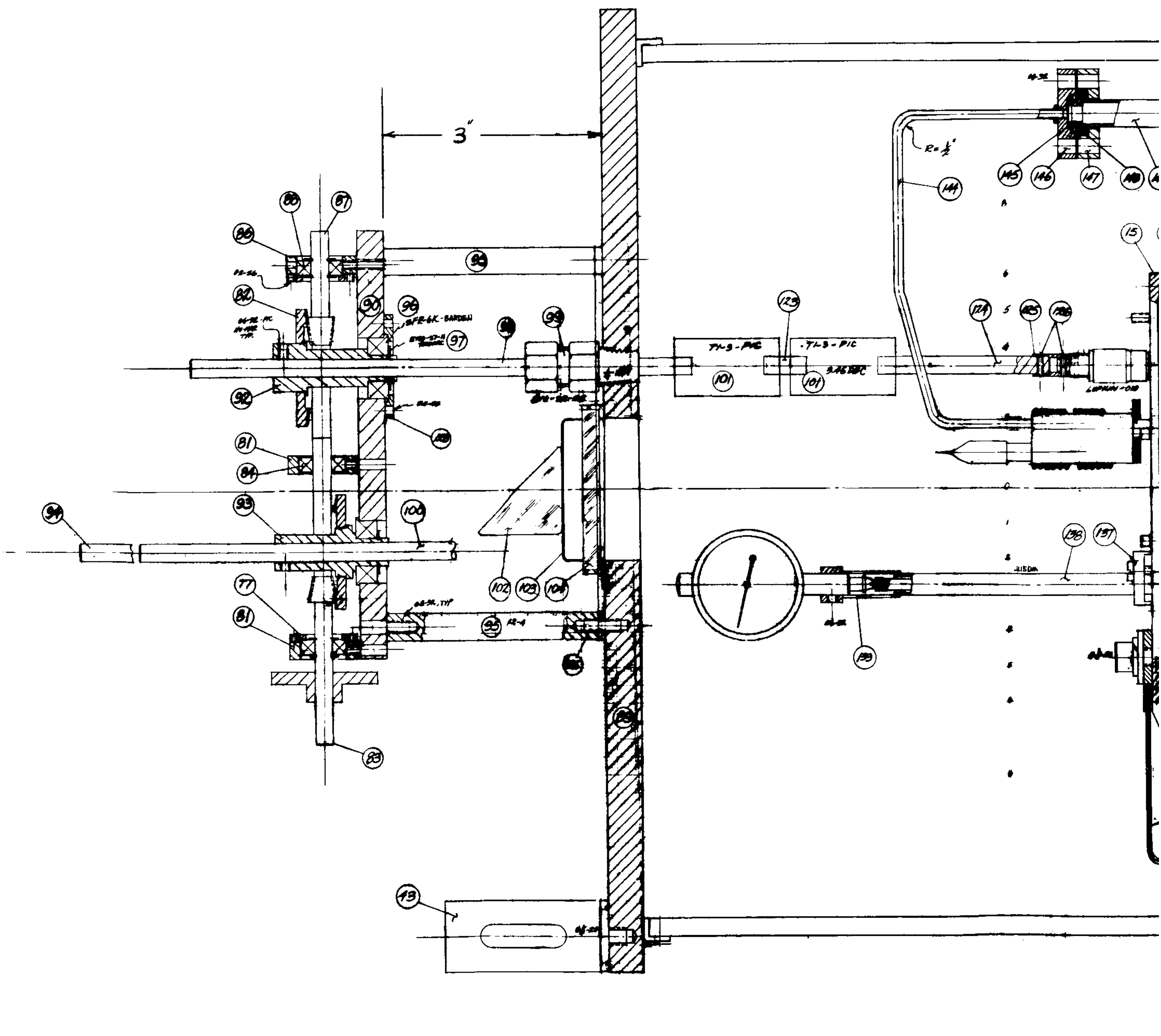

3"
R=1/2"
144
145
146
147
15
86
88
87
82
90
96
8FR-6K-BARDEN
97
99
123
TI-3-PIC
101
124
125
126
81
84
93
94
100
102
103
104
77
95
83
138
137
139
43

2

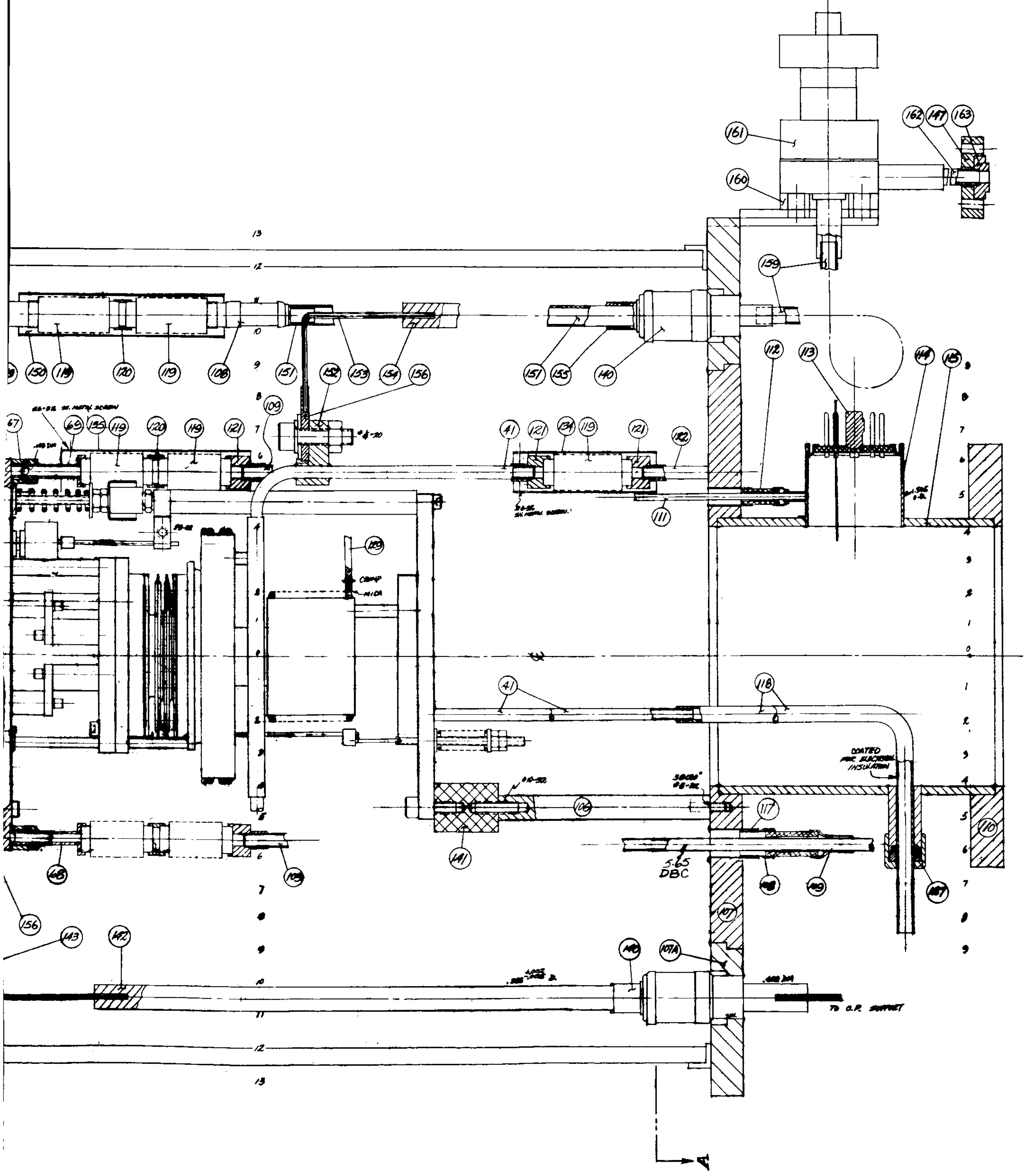

161
160
162
147
163
159
112
113
114
115
150
119
120
108
151
152
153
154
156
155
140
109
67
69
135
121
41
134
122
111
129
CRIMP
MICA
118
COATED
INSULATION
106
141
117
5.65 DBC
148
149
110
107
68
143
142
107A
TO O.P. SUPPORT
A

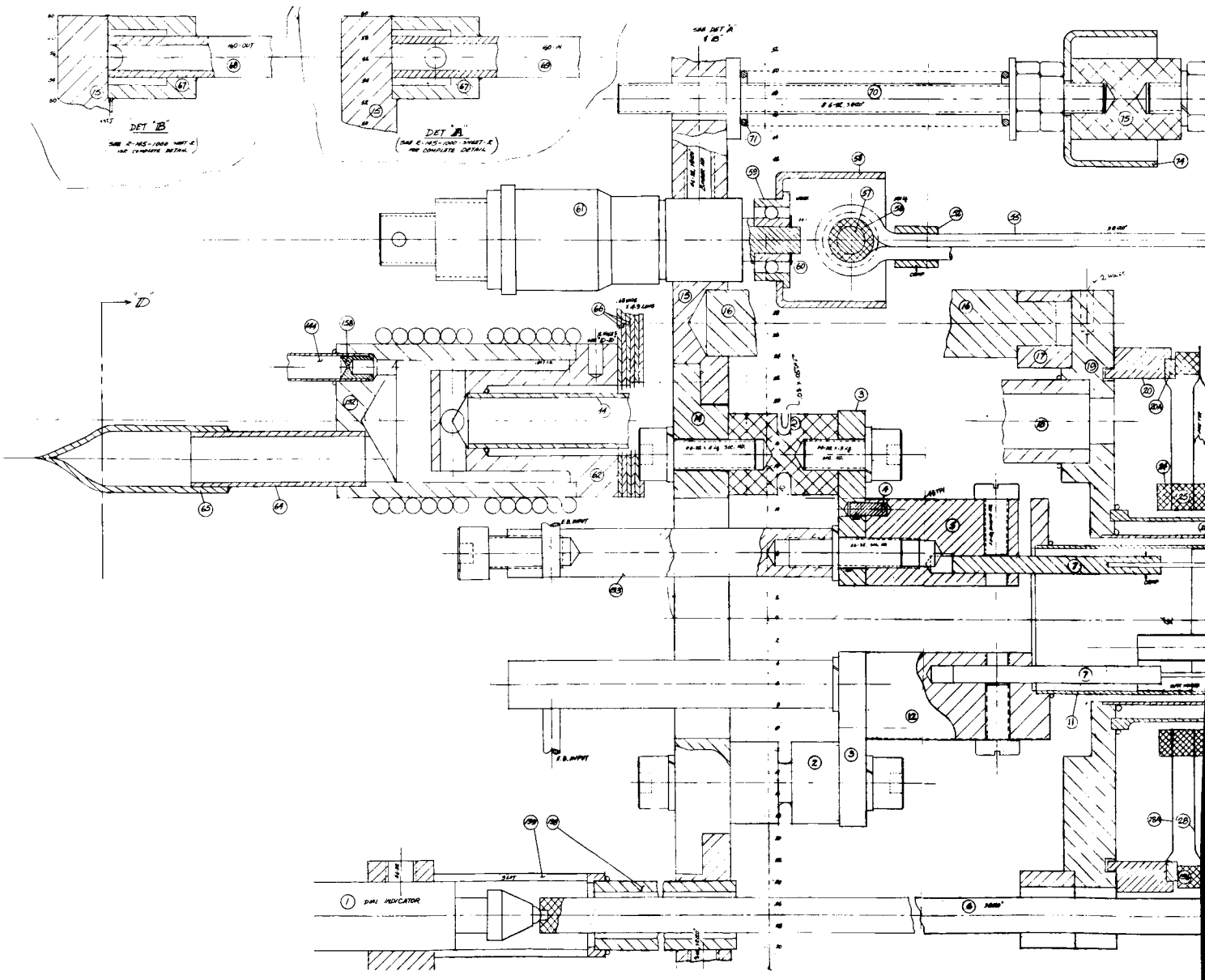
DET "B"
DET "A"
DIAL INDICATOR

2

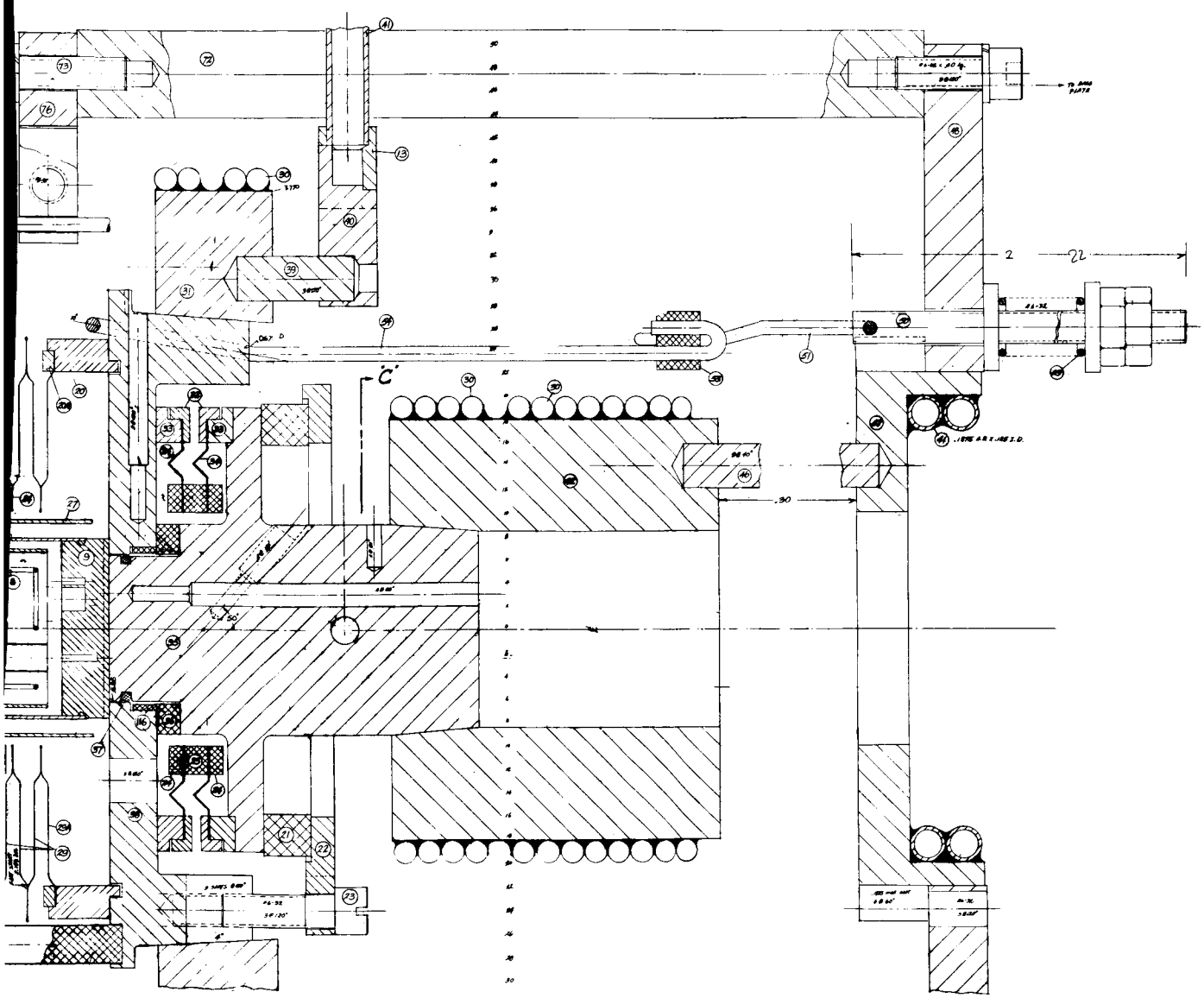

Figure II-2

Test Converter and Base Plate

TABLE OF NOMENCLATURE

for Figure II-2

1.	Dial Indicator	26.	Emitter Sleeve
2.	Insulator	27.	Emitter Shield
3.	Gun Holder	28.	Bellows Flanges
4.	Pin	28A.	
5.	Filament Support	29.	
6.	Sapphire Rod	29A.	
7.	Filament Lead	30.	Guard Ring Heater
8.	Filament	31.	Guard Ring Heater Block
9.	Emitter	32.	Flexible Flange Retainer
10.	Sight Pipe	33.	Flexible Flange Adapter
11.	Filament Shield	34.	Flexible Flange
12.	Shield Support	35.	Collector
13.	Guard Ring Cooler Adapter	36.	Collector - Guard Ring Spacer
14.	Gun Base	37.	Sapphire Balls
15.	Top Plate	38.	Guard Ring
16.	Top Plate Support Rod	39.	Guard Ring Heater Support Rod
17.	Top Plate Support Ring	40.	Guard Ring Cooler
18.	Cesium Reservoir Tubulation	41.	Water Tube
19.	Emitter Support Plate	42.	Collector Heater
20.	Bellows Adapter	43.	Pyrometer Support
20A.	Bellows Adapter Reinforcement	44.	Cesium Tubulation
21.	Insulator	45.	Thermocouple Wire
22.	Collector to Guard Compression Ring	46.	Collector Heater Support Rod
23.	Compression Screws	47.	Collector Cooling Plate
24.	Seal	48.	Support Plate
25.		49.	Spring

TABLE OF NOMENCLATURE

for Figure II-2 (continued)

50.	Tension Rod	76.	Tension Wire Clamp
51.	Tension Wire	77.	Anti-Backlash Plate
52.	Wire Retainer	78.	Gear
53.	Insulator	79.	Shaft
54.	Tension Wire	80.	Gear
55.	Tension Wire	81.	Plate
56.	Tension Wire Insulator	82.	Bevel Gear
57.	Rod	83.	Pinion
58.	Micrometer Adapter	84.	Bearing
59.	Ball Bearing	85.	Spring Retaining Washer
60.	Ball Bearing Retaining Washer	86.	Bearing Housing
61.	Micrometer	87.	Pinion
62.	Cesium Reservoir	88.	Bearing
63.	Cesium Reservoir Heater	89.	Top Plate
64.	Evacuation Tubulation Adapter	90.	Mechanism Support Plate
65.	Evacuation Tubulation	91.	Shaft Adapter
66.	Cooling Strap	92.	Gear Adapter
67.	Water Cooling Ring	93.	Gear Adapter
68.	Cooling Water Outlet	94.	Shaft
69.	Cooling Water Inlet	95.	Support Rod
70.	Guide Rod	96.	Bearing
71.	Compression Spring	97.	Bearing Retainer Washer
72.	Guide Rod Base	98.	Shaft
73.	Stud	99.	Gland
74.	Insulator Shade	100.	Shaft
75.	Insulator	101.	Bellows

TABLE OF NOMENCLATURE

for Figure II-2 (continued)

102. Prism
103. Prism Support Plate
104. Pyrex Window
105. Stud
106. Support Plate Rod
107. Base Plate
107A Base Plate Adapter
108. Water Feedthrough
109. Water Tube
110. Base Plate Lower Ring
111. Lead Wire
112. Lead Wire Feedthrough
113. Octal Plug
114. Octal Plug Adapter
115. Base Plate Neck
116. Sapphire Spacer
117. Leadthrough Adapter
118. Water Tube
119. Bellows
120. Bellows Adapter
121. Water Tube Adapter
122. Water Tube
123. Bellows Connector
124. Shaft
125. Micrometer Adapter
126. Roll Pins
127. Water Tube Coupling
128. Bearing Retainer
129. Heater Connectors
130. Gear
131. Shaft
132. Cesium Reservoir Heater
133. E. B. Filament Arms.
134. Bellows Retainer
135. Bellows Retainer
136. Ceramic Insulator
137. E. B. Gun Retainer
138. Dial Indicator Extension
139. Dial Indicator Holder
140. Emitter Output Leadthrough
141. Standoff
142. Emitter Output Lead
143. Output Strips
144. Inner Gas Inlet Tube
145. Copper Gasket
146. Vacuum Flange
147. Vacuum Flange
148. Flange Adapter
149. Flange Adapter Pipe
150. Bellows Retainer
151. Gas Inlet Pipe

TABLE OF NOMENCLATURE

for Figure II-2 (continued)

152. Guard Output Adapter
153. Output Strips
154. Guard Output Lead
155. Gas Pipe Adapter
156. Output Strip Adapter
157. Cesium Strip Connector
158. Cesium Restriction Plug
159. Flexible Tube
160. Valve Adapter
161. Inner Gas Inlet Valve
162. Valve Adapter Tube
163. Vacuum Flange Adapter

set to measure changes in the relative position of the emitter and collector structures.

A tubulation (No. 18) leads from the emitter support structure to the cesium reservoir (No. 62). A similar reservoir is used for the cesium fluoride. The only difference between the two is that the entrance to the tubulation leading to the cesium reservoir is restricted by a 10-mil orifice. This orifice prevents cesium fluoride vapor from condensing in the cesium reservoir at a rapid rate. In the case of the plasma-additive converter, inert gas is introduced by means of a tubulation (No. 144) leading from the cesium reservoir to the exterior of the vacuum envelope of the converter and to the inert-gas injection system.

For a description of the individual components of this device more detailed than the summary given above, the reader is referred to Reference 19. The changes which were made in the test vehicles used in the present program will now be outlined in detail.

1. BASE PLATE

To provide room for the inert-gas injection tubulation, the size of the glass bell jar around the converter was increased from 8 to 12 inches. This change required that the base plate diameter also be increased. A new ring (part No. 107A) was added to the old base plate (part No. 107). The two were welded as shown in Figure II-2. In this new ring, large feedthroughs (No. 140) were placed to allow for the passage of the inert gas injection tube (part No. 151) and the emitter current lead (part No. 142). The guard current lead (part No. 154) was also brought out of the bell jar in the same manner. An all-metal diaphragm valve (part No. 161) was added to the base plate to allow for the isolation of the interior of the converter from the gas injection system.

2. TOP PLATE

The top plate diameter had to be increased to allow the use of the larger bell jar. In this case new top plates were fabricated. An opening was provided in the center of the top plate which accommodates a Pyrex window (part No. 104); the emitter temperature observation prism (part No. 102) is located above this window. In the previous design this prism was located immediately above the emitter cooling ring (No. 15). With that arrangement the emitter black-body cavity had to be sighted through the Pyrex bell jar walls, and, since these walls have a certain amount of ripple, distortion of the black-body hole image always occurred to some extent. The present system eliminates any distortion whatsoever of the black body hole image, since it is viewed through a ripple-free window. Support for the pyrometer was also provided on the top plate by a bracket (part No. 43), and in this manner the pyrometer is fixed on the top plate permanently.

3. RELOCATION OF DIAL INDICATORS

The dial indicators (part No. 1) were relocated well above the emitter cooling plate through the use of an extension tube (part No. 138). This change was made because on some occasions in previous work the dial indicators were overheated by radiation from the emitter cavity. Overheating caused them to jam and necessitated their replacement. The present scheme assures satisfactory operation of these indicators.

4. CESIUM RESERVOIR

To allow the introduction of inert gas and the variation of its pressure, a tubulation was added to the cesium reservoir (part No. 144), as mentioned

above. The entrance to this tubulation is restricted by a 10-mil orifice so that the flow of cesium vapor through this orifice will be minimized. The cesium pressure will still be determined by the temperature of the liquid in the reservoir, since the liquid-gas interface area is much larger than the orifice area. Any cesium that does enter this tubulation will condense on its walls immediately beyond the restriction and will flow, because of gravity, back into the reservoir. The gas injection tubulation is equipped with a copper-gasket coupling (parts Nos. 146 and 147) which joins it to a larger tube (part No. 149). Two bellows (No. 119) allow relative motion between the emitter assembly and the base plate. A feedthrough (part No. 108) isolates electrically the part of the pipe that is at emitter potential from the remainder which is kept at ground potential. After coming through the base plate through the feedthrough (part No. 140), that pipe leads to an all-metal valve (part No. 161). Another coupling (part No. 147-163) allows the joining of this portion of the gas injection system with the remainder described below.

5. GAS INJECTION SYSTEM

A system of introducing inert gas and measuring its pressure was designed and fabricated. A schematic of this system is shown in Figure II-3. A No. 4 cylinder of high-purity gas is used as the primary supply of inert gas. A two-stage regulator attached to the cylinder allows dropping the pressure from 250 psi to about 10 psi in charging the 75-mm cylinder. The 75-mm cylinder is used as a supply of gas for a third cylinder, the capacity of which is 500 mm. Directly to this cylinder is connected a diaphragm-type manometer, which measures its pressure continuously. The last two cylinders are separated by a micro-flow valve which allows

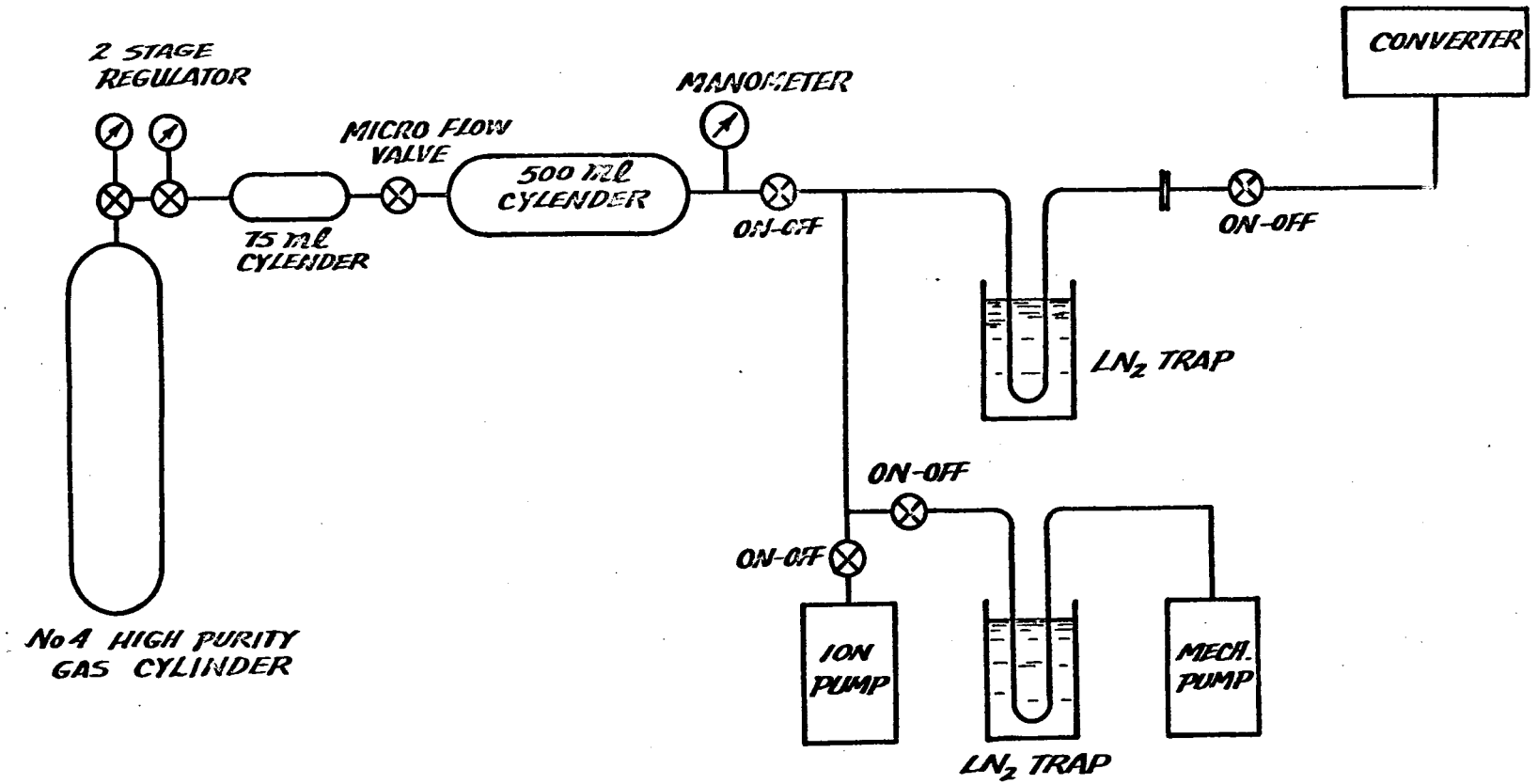

Figure II-3. Schematic of Inert-Gas Injection System

the bleeding of gas from the small cylinder into the large one. The characteristic of this valve is shown in Figure II-4. By using this valve the 500-mm cylinder can be charged from 0.2 mm of mercury absolute pressure up to 100 mm. Downstream of the last cylinder is an ON-OFF all-metal valve which allows the isolation of the last gas reservoir from the converter and the pumping system. The pumping system consists of an ion pump, which also can be isolated by an ON-OFF valve, and a mechanical pump used for roughing either the converter or the entire system before starting the ion pump. A liquid nitrogen trap is provided upstream of the mechanical pump so that any oil vapor flowing back into the system from it will be trapped. The system has one additional isolating ON-OFF valve located on the base plate described above. A liquid nitrogen trap is again provided between the converter and the remainder of the system. This trap prevents contamination of the converter by the gas injection system and the flow of cesium from the converter into the gas system. Two complete gas injection systems have been assembled, one for the tungsten device and one for the rhenium device, and both are presently operational.

6. OPTICAL PYROMETER

No changes were made in the instrumentation described in Reference 19 except for the optical pyrometer. The lens system of the standard Leeds and Northrop pyrometer was modified so that the image of the 0.032" blackbody cavity on the emitter is larger then five times the filament width. This change is aimed at improving the emitter temperature measurement accuracy. One modified pyrometer was calibrated by Leeds and Northrop and is in use. A second instrument is awaiting calibration by the Bureau of Standards against a primary standard.

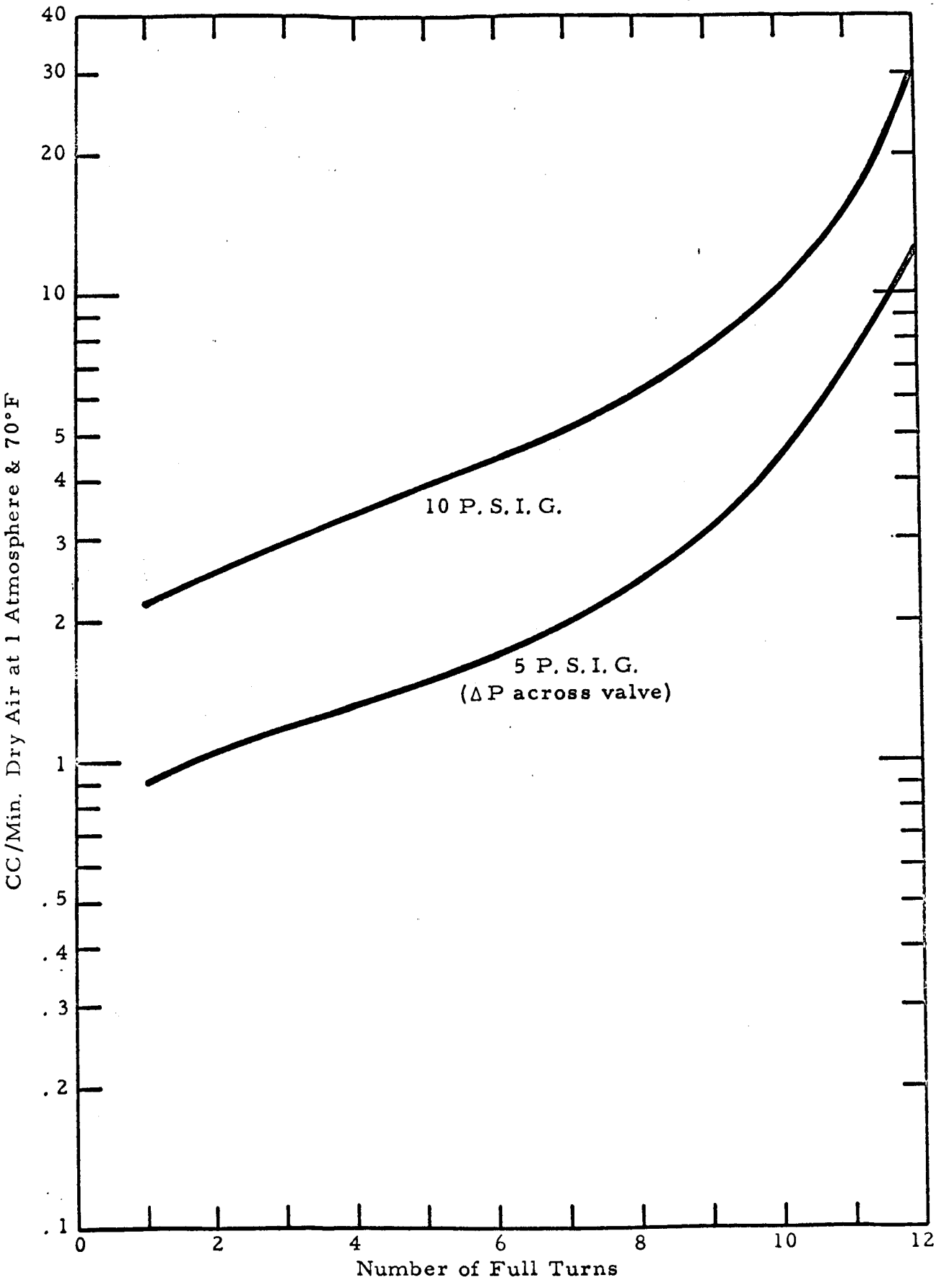

Figure II-4. Characteristic of Microflow Valve.

CHAPTER III

SELECTION OF GAS ADDITIVE

Electron currents in thermionic diodes are attenuated by two processes. The first is formation of electron space charge in the interelectrode spacing, which results in buildup of potential barriers for electrons.

The second process is scattering of electrons. Electron space charge in cesium diodes can be neutralized by the cesium ions that are produced in the discharge. These ions, however, are short-lived in the interelectrode spacing due to leakage out of the boundaries and they must be continuously generated to maintain a steady density in the plasma. Loss of the ions due to leakage can be reduced appreciably if the diffusivity of the ions is decreased. This can be achieved by addition of a gas to provide scattering centers for the ions. Most of the gases that have a high scattering cross section for cesium ions also attenuate electron current. Inert gases, however, are an exception to this rule because of the Ramsauer Effect. These gases have a high scattering cross section for ions, but at operating electron temperatures their scattering cross section for electrons is very small. Hence addition of an inert gas to the plasma is expected to preserve the ions while leaving electron current virtually unaffected.

An extensive literature survey has been made to determine the best values of transport parameters of electrons and cesium ions in inert gases. The object of this survey was to select a gas which has a high scattering cross section for cesium ions and a low cross section for electron scattering. The survey was mainly concentrated in the periods 1928-1935 and 1961-1964, when a great deal of work was done on this problem. The period

in between was covered by the references from the papers in the above periods and also from survey papers which were written by various authors. A list of the important references is included in this report. The electron or ion current that will be attenuated due to scattering by inert gases will be derived from the kinetic theory of gases and the diffusion equation for long and short mean free path, respectively.

$$\frac{J}{J^*} = e^{-d/\lambda} \qquad \text{for} \qquad \frac{d}{\lambda} << 1$$

$$\frac{J}{J^*} = \frac{1}{1 + \frac{3}{4}\frac{d}{\lambda}} \qquad \text{for} \qquad \frac{d}{\lambda} >> 1$$

J = attenuated current of ions or electrons

J^* = incident current of ions or electrons

d = interelectrode spacing

λ = electron or ion mean free path

For selection of the values of the mean free paths needed for these calculations, the values obtained by various authors were compared, and those which seemed to be most dependable were chosen. The values of electron mean free path in A, Kr and Xe were calculated from the values of absorption coefficient reported by Ramsauer and Kollath[1], since their work was confirmed by others.

A report by DeVoto[3] has compiled the reported data on electron cross section in Argon. His theoretical values are in good agreement with the work by Ramsauer and Kollath. The mean free path of cesium ions in Kr and Xe was calculated from the values of mobility reported by Powell and Brada[3] and for argon from Chanin and Biondi[4]. Ramsauer and Kollath

give the following absorption coefficients for 0.5 eV electrons in inert gases:

	cm^2/cm^3 of vapor at 0°C and 1 torr
Ar	1
Kr	2
Xe	5

Absorption coefficient is, in effect, a macroscopic cross section, or

$$\alpha = n_o \sigma$$

where n_o is the particle density at 0°C and 1 torr.

$$n_o = 3.5 \times 10^{16} \text{ particles/cm}^3$$

and

$$\lambda = \frac{1}{n\sigma}$$

For average gas temperature of 1000°K, $n = 0.98 \times 10^{16}$ particles/cm^3.

$\therefore \lambda$ can be calculated from the following equation:

$$\lambda = \frac{1}{\alpha} \frac{n_o}{n}$$

Mobility and diffusion coefficient are related by

$$\mu = \frac{eD}{kT}$$

where μ = the mobility of ions in cm^2/sec volt

D = diffusion coefficient in cm^2/sec

$\frac{e}{kT}$ = average gas temperature in electron volts

Diffusion coefficient, in turn, is related to mean free path by

$$D = \frac{v\lambda}{3}$$

where v is the velocity of the particles in cm/sec.

The mobility of Cs ions in Kr and Xe is given by Powell and Brada at one atmosphere of pressure:

	μ $cm^2/sec\ volt$
Kr	1.4
Xe	1

The value for argon is given by Chanin and Brondi at one atmosphere:

$$\mu = 2\ cm^2/sec\ volt.$$

Converting these values to mean free path and calculating their effect on attenuation of electrons and cesium atoms at 1 torr pressure and 1000°K average gas temperature for a 10-mil interelectrode spacing, Table I is obtained. From examination of this table, it is evident that the appropriate inert gas that can reduce the ion current appreciably, and is transparent to electrons, is argon.

TABLE I

EFFECT OF ADDITION OF 1 TORR OF INERT GASES
IN A 10-MIL-SPACING PLASMA AT 1000°K

Inert Gas	λ_i, mils	λ_e, mils	$\frac{J_i}{J_i^*} = \frac{1}{1+\frac{3}{4}\frac{d}{\lambda_i}}$	$\frac{J_e}{J_e^*} = e^{-d/\lambda_e}$	Ion Current Attenuated by	Electron Current Attenuated by
A	4.2	1400	0.36	0.993	64%	0.7%
Kr	2.9	700	0.28	0.986	72%	1.4%
Xe	1	280	0.22	0.968	78%	3.2%

CHAPTER IV

EMITTER PREPARATION AND EXAMINATION

The experimental work using cesium fluoride additive is conducted in a tungsten-emitter converter. The inert gas additive experiments use two converters, one tungsten-emitter and one rhenium. To fulfill the above requirements two tungsten emitters and one rhenium were prepared initially. One more emitter of each kind will be prepared shortly to serve as backups to avoid a long interruption in the program in case of an accidental failure of a test converter.

In this chapter the composition, preparation and definition of each kind of surface are given. The results of electron microscopy and x-ray orientation examinations of tungsten and rhenium surfaces prepared in the fashion described here will be given in a later report.

1. TUNGSTEN

Two polycrystalline tungsten emitters have been prepared with electropolished and heat-treated surfaces. These have TEECO designations W9 and W10.

a. Materials

Wrought sheet stock was used for the tungsten emitters. The manufacturer supplied, and certified, the following spectroscopic analysis: (all units ppm).

Al < 6	Fe 13	Mn < 6	Mo 30
Ca < 3	Ni 8	Mg < 3	Co 29
Si 50	Cu <3	Sn < 6	Zr < 3

b. Surface Preparation

The stock had a good ground surface. After electrical discharge machining to shape, the emitters were cleaned, and electropolished in 5% aqueous sodium hydroxide solution at a potential of 10 volts for about 30 seconds. The resulting surfaces were photographed, and typical areas are shown in Figures IV-1 and IV-2. Slightly different polishing rates on adjacent grains make some boundaries prominent, while small pits are also visible.

c. Heat Treatment

Each emitter was heated by electron bombardment in a cold-walled vacuum furnace for 1 hour 5 minutes at 2300°C. The temperature was read with an optical pyrometer (0.65 μ) and is corrected for the emissivity of tungsten. The pressure was determined from the current in the Vac Ion pump used to evacuate the system, and found to be less than 1×10^{-6} torr while the specimen was at temperature. The heat treatment was chosen to duplicate that used on W4 and W6 in Task IV of this contract.

d. Examination of Emitter Surfaces

After heat treatment the surfaces were again photomicrographed, and typical areas are shown in Figures IV-3 and IV-4. Grain growth and grain boundary grooving have occurred, as expected. The new grain structure is clearly delineated by the grain boundary grooves, while faint traces of the old grain structure are visible, especially on Figure IV-4.

Electropolishing tends to produce "roll-off" or rounding at the edge of a specimen, and, in order to study this, interference fringe patterns were made at the edge of each emitter using sodium yellow light. Figures IV-5 and IV-6 are composite photographs of typical areas at the edge of emitters

Figure IV-1. Emitter W9 after Electropolishing, 310x.

Figure IV-2. Emitter W10 after Electropolishing, 310x.

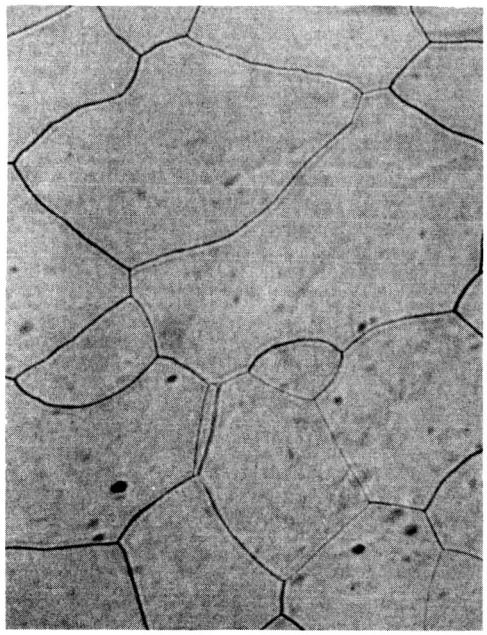

Figure IV-3. Emitter W9 after Heat Treatment, 310x.

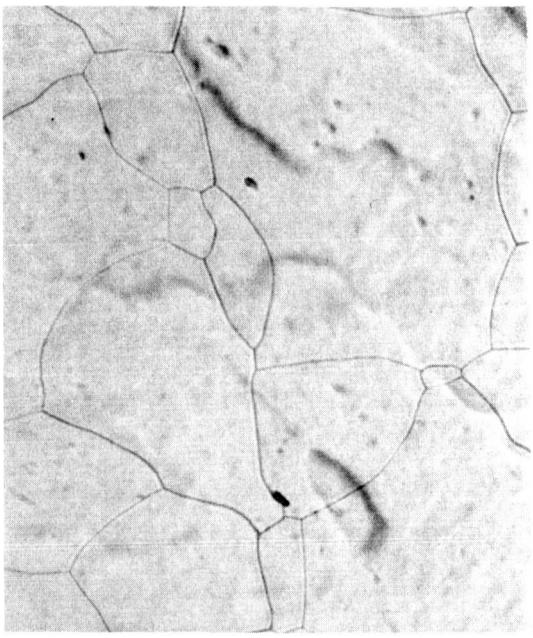

Figure IV-4. Emitter W10 after Heat Treatment, 310x.

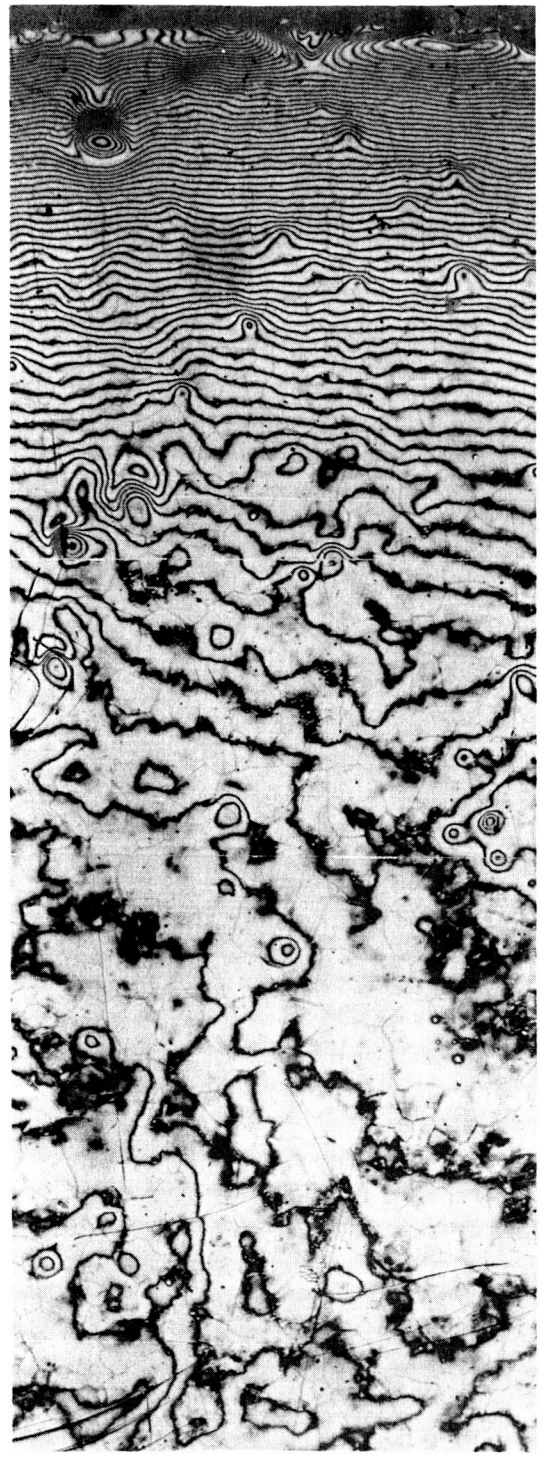

Figure IV-5. Interference Fringe Pattern from W9 after Heat Treatment, Showing Edge, 74x.

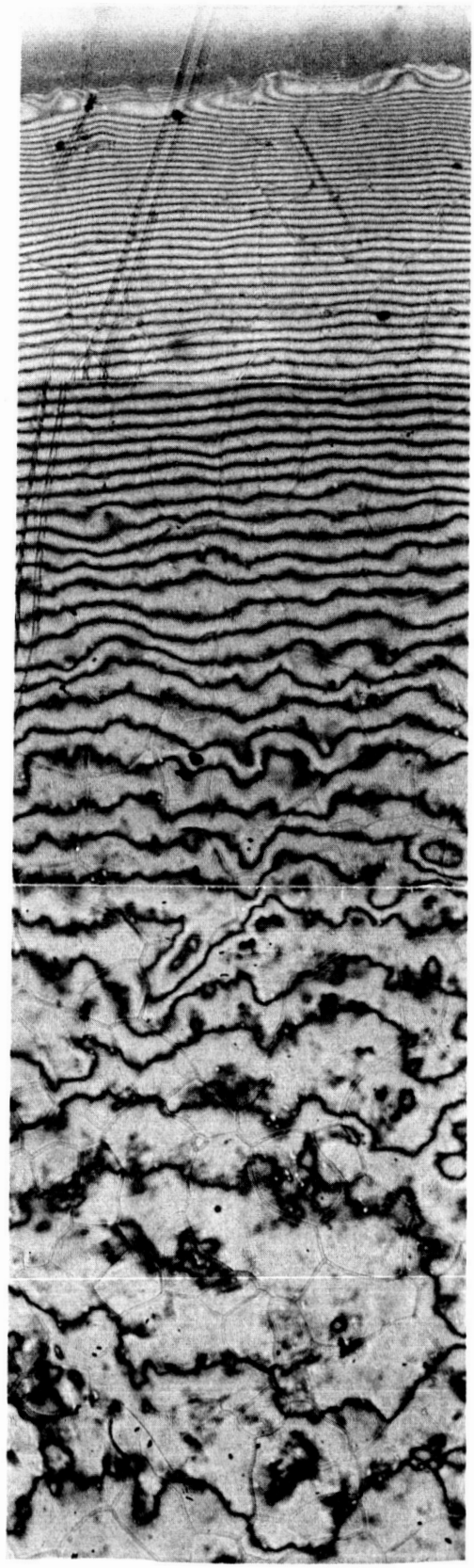

Figure IV-6. Interference Fringe Pattern from W10 after Heat Treatment, Showing Edge, 152x.

W9 and W10 at 74X and 150X respectively. The "roll-off" is manifest as rows of increasingly close-spaced fringes parallel and close to the edge of the emitter. Measurements on these, taking the magnification into account, show that the "roll-off" is completely confined within 0.04" of the edge of the emitter. This area faces the guard ring in the converter, and therefore will not in any way affect the converter performance. More detailed visual examination showed:

1. that the photographed areas were typical, and in no area was the roll-off width likely to approach the guard ring width;

2. that the inner areas of each composite photograph are typical of the central parts of the emitters, which show no steep gradients (except at a few polishing defects, such as that in Figure IV-7, which is about 7 mils across and 1/4 mil deep) and are flat to within a micron or so.

e. Conclusions

These emitter surfaces have behaved exactly as is predicted from our considerable experience with tungsten surfaces, and are expected to be completely stable during diode operation.

2. RHENIUM

One polycrystalline rhenium emitter has been prepared with an electroetched and heat-treated surface. This has the TEECO designation Re 31.

a. Materials

Wrought sheet stock was used for the rhenium emitter. The manufacturer supplied and certified the following spectroscopic analysis

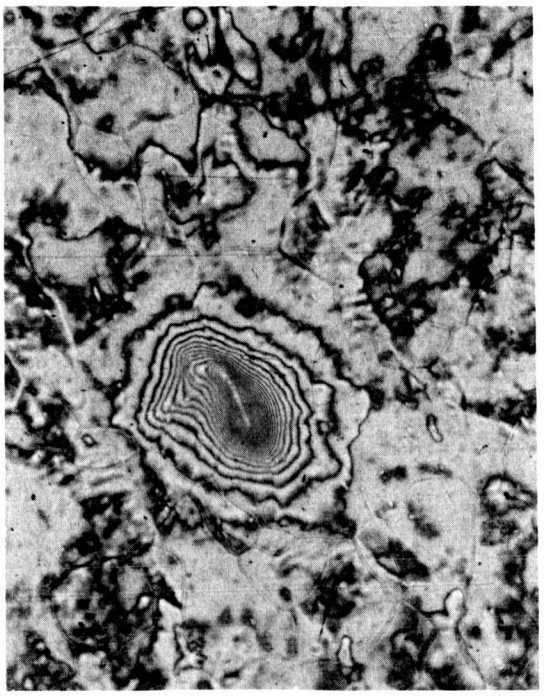

Figure IV-7. Interference Fringe Pattern from W10, Showing Polishing Defect, 152x.

(all units ppm):

Al < 1	Cu < 1	Fe 43	Mg < 1	Si < 1

Ag B Be Mn Mo Na Nb Pb Sn Th Ta V Zr W sought but not detected.

b. Surface Preparation

The surfaces were ground flat and parallel, and the slug was annealed for 2.8 hrs at 2350°C in a cold-walled furnace. It was then shaped by electrical discharge machining, and electropolished in the usual perchloric acid/alcohol mixture at 22 volts (9 amps) for about 20 seconds. It was next electroetched in the same electrolyte at 5 volts (1.6 amps) for 80 secs. The resulting surface was photographed, and typical areas are shown in Figures IV-8 and IV-9. The differential etching rate removes some grains much faster than others, so that they are not all in focus on the photomicrograph.

c. Heat Treatment

The emitter was heated in the cold-walled furnace for 3 hours at 2420°C. The temperature was read with an optical pyrometer, and is corrected for the emissivity of rhenium. The pressure at the Vac Ion pump was found to be less than 1×10^{-6} torr while the specimen was at temperature. The heat treatment was designed to duplicate that used on Re 15 and Re 16 in Task IV of this contract.

d. Examination of Emitter Surface

After this heat-treatment the surface was again photomicrographed, and typical areas are shown in Figures IV-10 and IV-11. Only slight traces of grain boundary movement are visible, because the specimen had an anneal prior to surface preparation and heat treatment. The etched

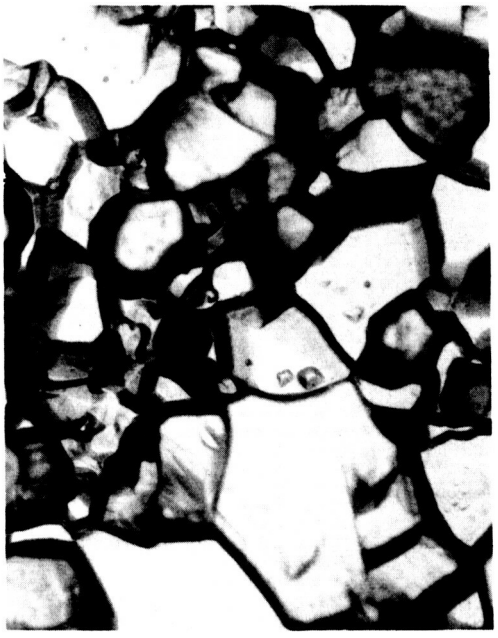

Figure IV-8. Emitter Re31 after Electroetching, 310x.

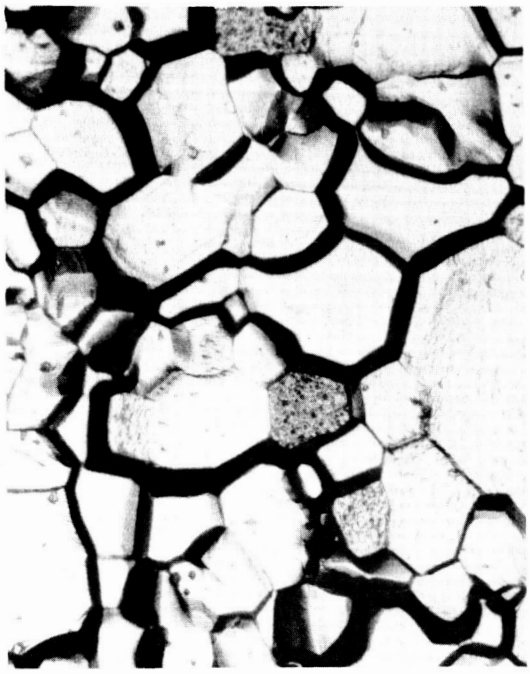

Figure IV-9. Another Area of Re31, 310x.

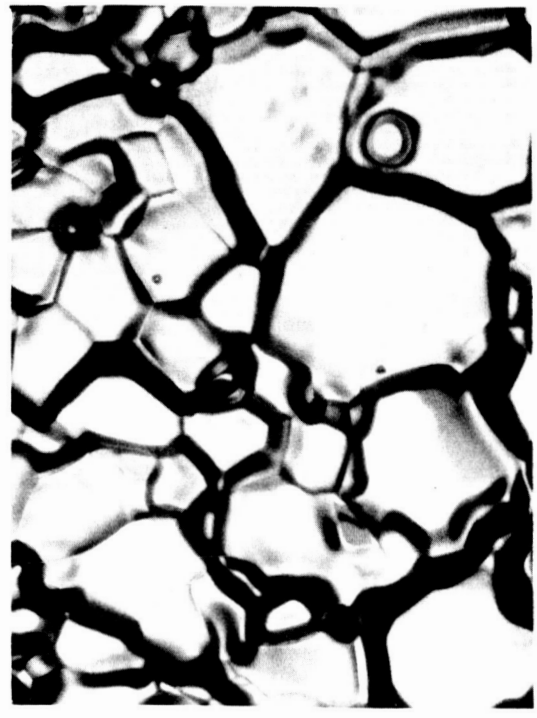

Figure IV-10. Re31 after Heat Treatment, 310x.

Figure IV-11. Another Area of Re31, 310x.

grain boundaries, which have well defined sharp edges in Figures IV-8 and IV-9 have, as expected, become rounded by the heat treatment. Two small thermally etched flat surfaces are visible on Figure IV-10 — one at the center and one near a corner. These are commonly observed following heat treatment of an etched surface. The smoothing effect has extended to the surfaces of the grains which had a textured appearance in Figures IV-8 and IV-9.

The surfaces of this emitter are too rough to produce meaningful interference fringe patterns, and so no detailed study of "roll-off" is possible. However, there is no reason to doubt that it is confined to a narrow band at the edge, just as it is in tungsten. In any case the "roughness", or depression of some grains below their neighbors, is probably greater than any roll-off.

e. Conclusions

This emitter surface behaved exactly as is predicted from our considerable experience with rhenium surfaces, and it is expected to be completely stable during diode operation.

3. GENERAL

One more emitter each of rhenium and tungsten will be prepared shortly, to use as backup parts in case of failure. The tungsten emitter will be examined with an electron microscope. An attempt will be made to examine the etched rhenium emitter the same way, but it is likely that the roughness of the surface will prevent making the necessary replica of it.

CHAPTER V

TUNGSTEN WORK FUNCTION

The work function measurements conducted on the tungsten emitter surface to date have covered vacuum emission and emission in the presence of cesium fluoride. The vacuum emission experiments are now completed, while the measurements with CsF are only in the initial stages. The experimental procedure used in acquiring the data, the experimental results, and their correlation are presented in the following paragraphs.

1. EXPERIMENTAL PROCEDURE

Emitter work function values are determined from saturated emission measurements, using the Richardson Equation. The experimental task, then, consists of obtaining current-voltage characteristics at known emitter temperatures. The instrumentation used for this task is shown in Figure V-1. This equipment allows tracing of the current-voltage characteristic manually by varying the output of power supply P_1. The function of power supply P_2 is to maintain the collector and guard-ring voltages within 2mV of each other. A series of shunt resistors, 0.5Ω to 5KΩ, generate the current signal for the Y axis of an X-Y plotter. The voltage signal is fed directly from voltage taps on the emitter and collector to the X axis of the X-Y plotter. A detailed description of the electronics shown in Figure V-1 is given in Reference 19.

After the proper instrumentation is connected to the test converter, the emitter and collector surfaces are made parallel to each other. In practice, the emitter is made parallel to the collector by individual

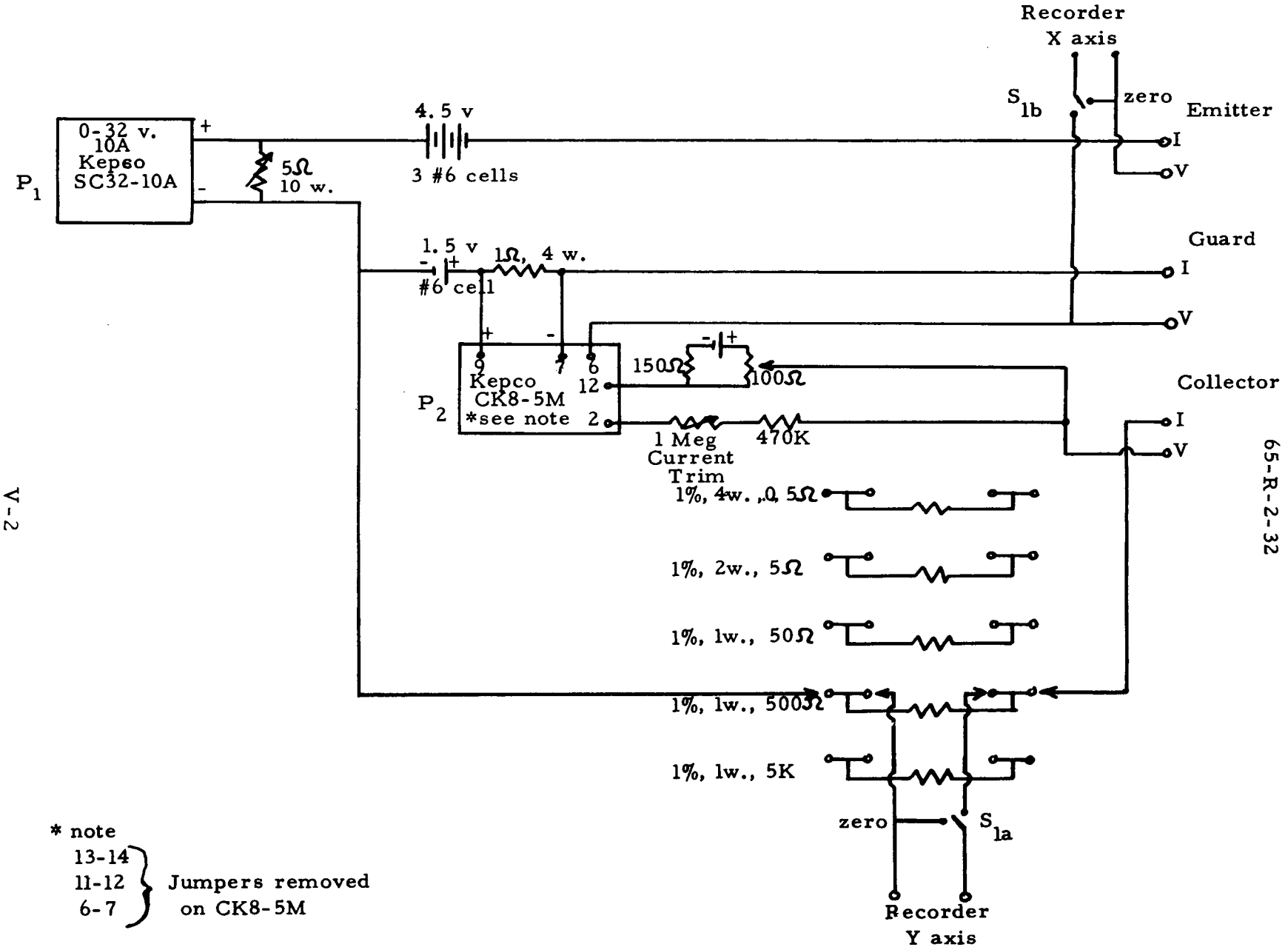

Figure V-1 . Schematic of Quasi-Static Test Panel.

adjustment of the three spacing micrometers. The procedure is essentially a trial-and-error process. Adjustments are made so that the J-V characteristic can be made as "ideal" as possible, i.e., the knee of the curve is as sharp as possible, without shorting. When parallelism is accomplished the emitter shorts to the collector without shorting to the guard ring. All three micrometer drive shafts are then geared together and are driven simultaneously thereafter.

For emitter work function measurements the collector and guard ring are kept quite cold, around 300°C for vacuum measurements and 50°above the additive reservoir temperature for additive work function measurements. The spacing is kept at its minimum value, approximately 0.5 mil. The purpose of this is to avoid the presence of negative space charge, which would result in an erroneous saturation current measurement. The absence of space charge is ascertained by varying the spacing and observing that the saturation current remains virtually constant:

$$\left.\frac{\partial J_s}{\partial d}\right|_{T_E} = 0 \quad \text{as } d \to 0 \qquad (1)$$

where J_s is the saturation current, d the spacing and T_E the emitter temperature. Note that condition (1) does not necessarily hold true when Cs vapor is present because of scattering. Once all the above conditions are fulfilled, J-V characteristics are traced at selected emitter temperatures.

2. ADDITIVE TEST VEHICLE CHARGING AND OUTGASSING

Prior to outgassing, the tube was flushed with dry argon through the Cs reservoir tubulation. Twelve CsF pellets totaling approximately

0.6 g were dropped into the reservoir. The sealed metal Cs capsule was inserted into the reservoir tubulation, which was then pinched off. Outgassing was accomplished through the additive tubulation in a similar manner to that used in other test vehicles. A one-liter-per-second ion pump was connected to the additive tubing and left pumping after preliminary outgassing.

In order to avoid the significant loss of CsF during outgassing, the reservoir was maintained at or below 200°C for most of the outgassing period of 48 hours. For a total of three hours the CsF was outgassed at 300°C. Following this schedule was expected to result in a minimum loss of additive while still achieving sufficient outgassing. A final pressure of about 3×10^{-7} torr was attained before leak-checking and pinching off.

3. EXPERIMENTAL RESULTS

The saturation current values obtained from these tests have been plotted as a function of reciprocal emitter temperature. On such a plot work functions are associated with a set of roughly parallel diagonal straight lines. Any variation in work function with emitter temperature is shown when the data points cross these lines.

Before raising the additive reservoir temperature, the emitter was tested for bare work function. The values obtained are shown as +'s in Figure V-2. Initial readings were taken starting at a temperature of 1900°K and increasing to 2140°K. As the emitter was then cooled to 1830°K, additional readings were taken. For these runs the spacing was about 7 mils. From the plot it is seen that the initial values (4.85) were somewhat higher than expected for bare tungsten, but, as the above cycle was carried out, the values centered on 4.75 eV and remained there on

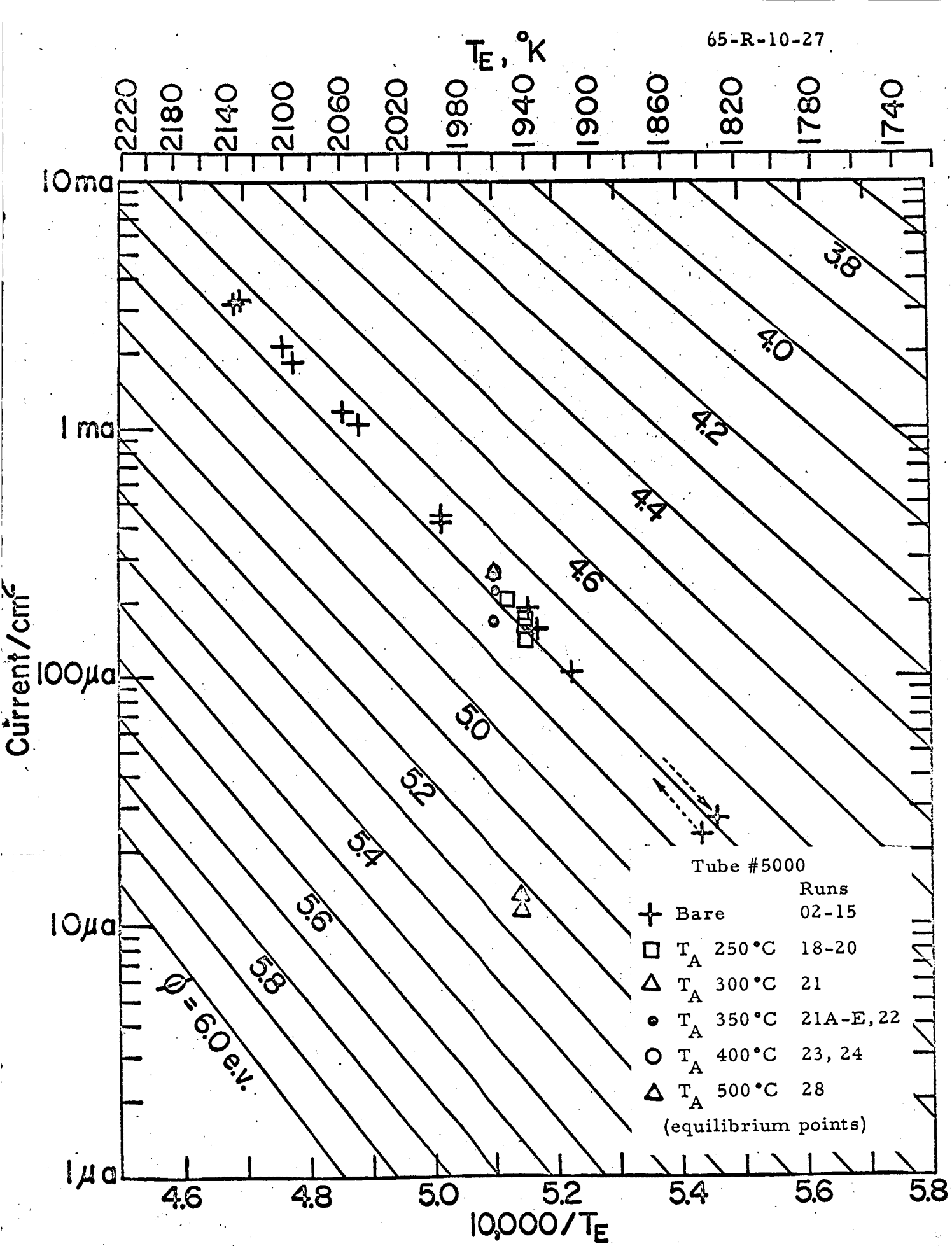

Figure V-2. Saturation Current vs Reciprocal Emitter Temperature for Bare Surface.

cooling. Additive probably coated the emitter somewhat during outgassing and was finally driven off at the higher temperatures. The bare surface value then remained, even during the cooler portion of the test.

To verify that space-charge effects were not influencing the results, a variable-spacing run was taken at a T_E of 2090°K, the region where these effects become significant. Figure V-3 shows the J-V characteristics obtained. At less than 7 mils the effect becomes negligible, as evidenced by the fact that the saturation current does not vary with spacing.

The additive reservoir temperature was progressively increased from 200°C in steps of 50°C until 400°C was reached. Both before and after allowing an overnight equilibrating time, J-V plots were taken and the work function calculated. No change from the bare values was observed. Figure V-2 is a plot of these results.

Increasing the reservoir temperature further to 500°C produced a pronounced change in saturation currents. After an initial overnight soak, the work-function-vs-emitter-temperature plot shown in Figure V-4 was made. The work function varies from 5.5 to 5.0 eV over the range of T_E from 1900°K to 2150°K as compared with the "bare" value of 4.75 eV. This is a significant effect which could be reproduced. When the device was cooled overnight and reheated to the same temperature, except for the CsF reservoir, which was kept cooled, the work function returned to its bare value. This change took approximately two hours. Upon raising the CsF temperature, the 5.4-eV level was reproduced.

There is apparently a variation in work function with additive coverage, since the higher-emitter-temperature points tend to approach the bare surface, while the low-temperature ones show increased additive effect.

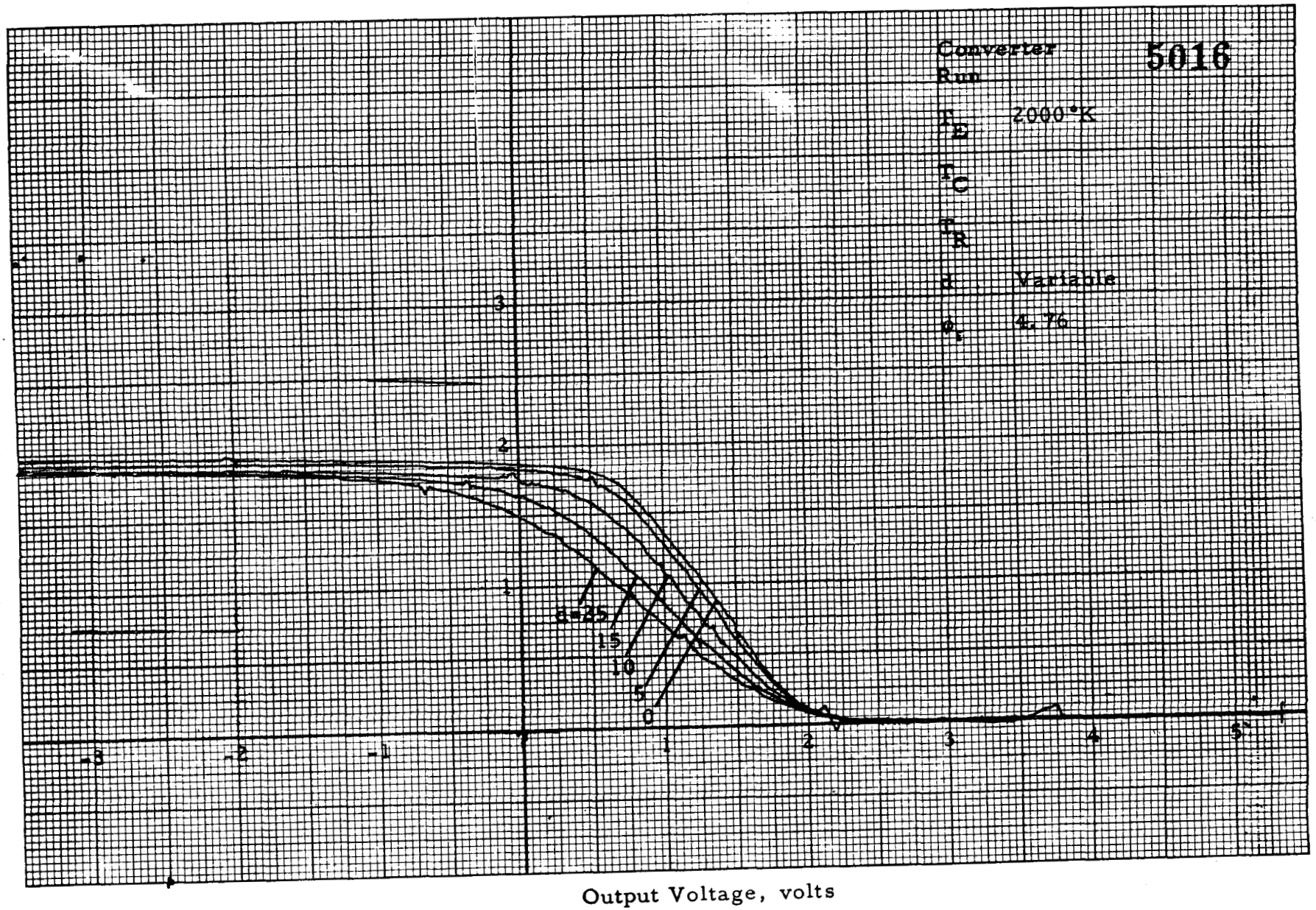

Figure V-3 Variable-Spacing Current-Voltage Family.

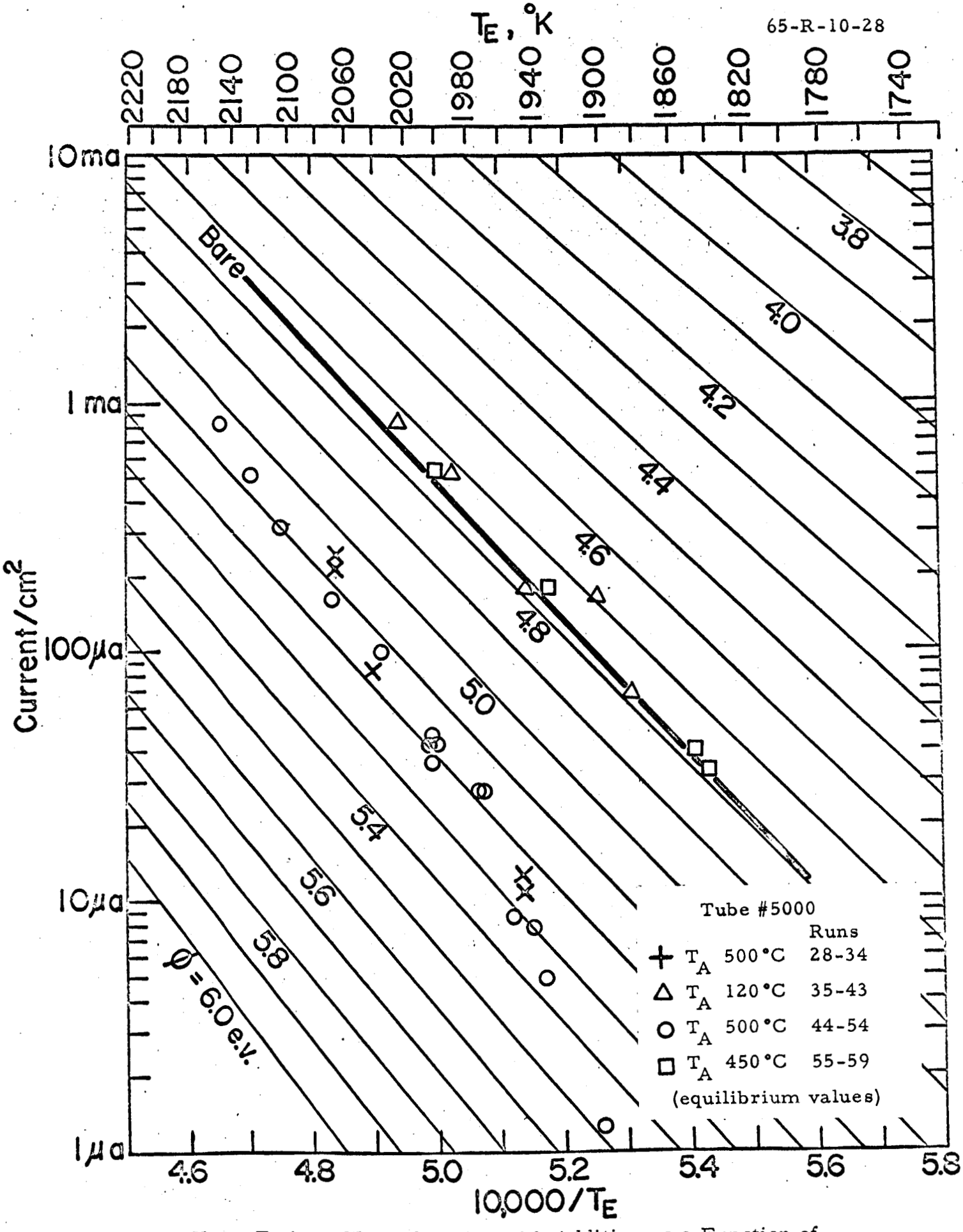

Figure V-4. Emitter Work Function with Additive as a Function of Emitter Temperature.

Each time the collector structure was heated a transient additive effect was observed. A large increase in work function occurred initially, which then decayed to the normal value for that reservoir temperature. In some cases an overnight period was required for this equilibrium to occur.

A higher-CsF-temperature (550°C) run did not produce results consistent with the previous data. In this case the fluoride produced an initial large increase in ϕ_E, from 5.1 to 5.3 eV at 2040°K, and then, when T_E was increased to 2110°K, the effect started to disappear. After an overnight period the work function had changed from 5.2 eV to 4.9 eV. Cooling the emitter to 1970°K resulted in a ϕ_E of 4.95 eV. These results are shown in Figure V-5. No equilibrating time has been allowed at these conditions up to this time. Since these runs were taken at a higher collector temperature than was used earlier, it is possible that a new reaction has taken place. Additional testing will be required to clarify this behavior.

A large back current similar to that observed in earlier work was present during most of the additive testing. Figure V-6 is a typical J-V curve showing this current. There is apparently a large ion current component present, as is shown by the non-saturation of this portion of the characteristic. In some cases these currents became large enough to limit testing to emitter currents above 10 μA.

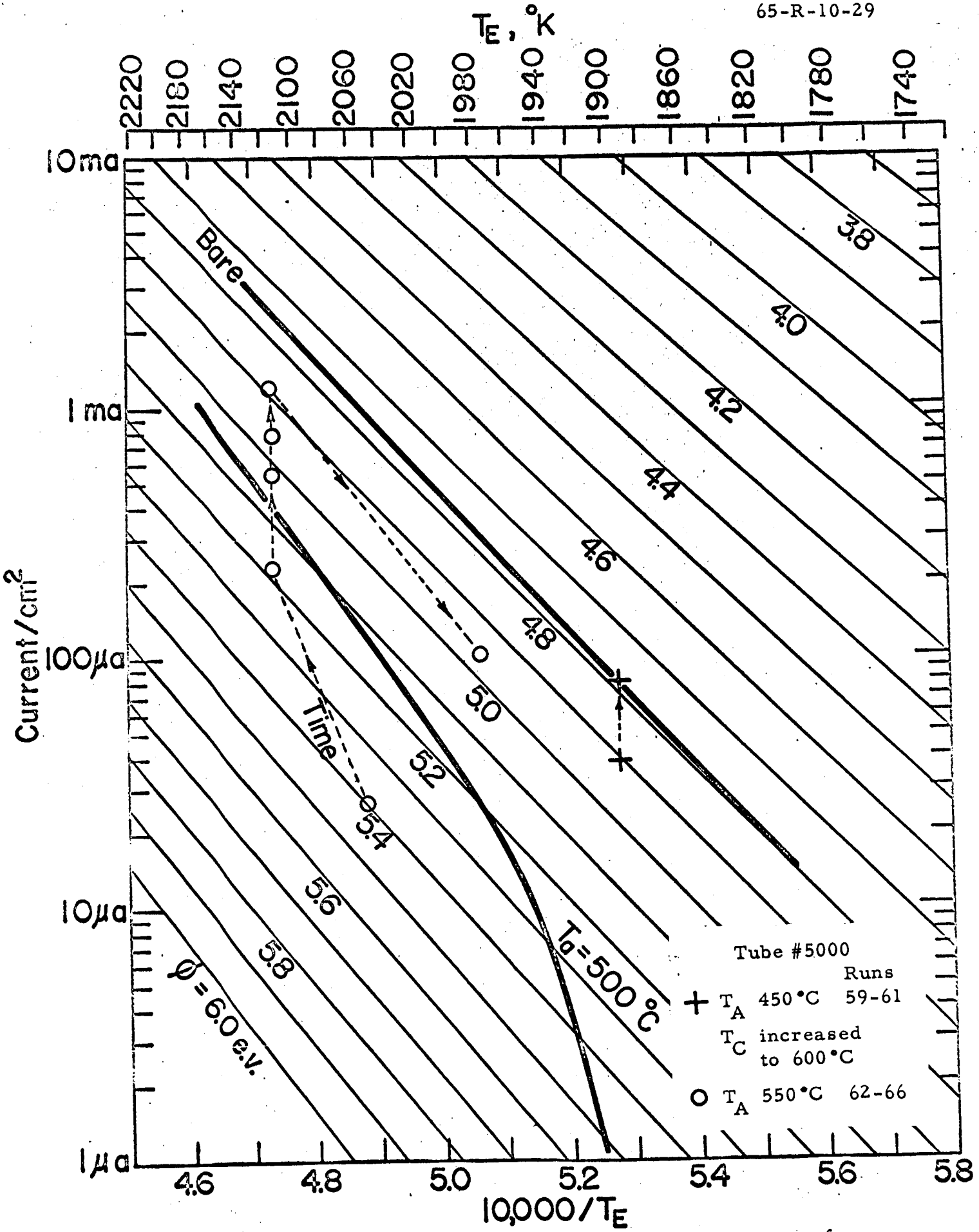

Figure V-5. Emitter Work Function with Additive as a Function of Emitter Temperature at Higher Additive Pressure.

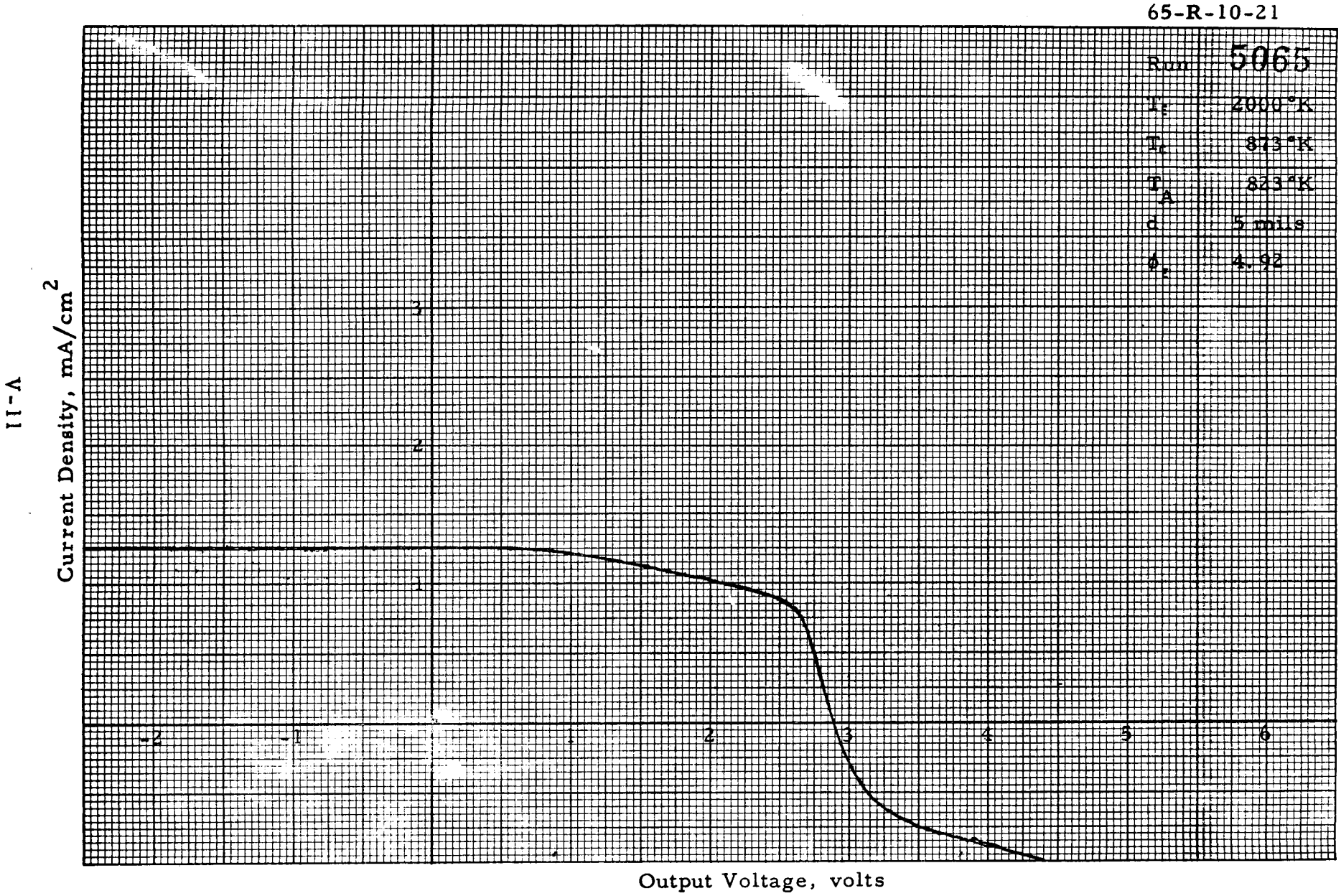

Figure V-6. Typical Current-Voltage Curve, showing Large Back Current.

CHAPTER VI

RHENIUM EMITTER WORK FUNCTION

The schedule of the experimental work with plasma additives (inert gas) calls for the measurement of emitter work function so that the surface can be defined prior to experiments with inert gases. The bare work function of the rhenium surface is measured first, followed by work function measurements in the presence of cesium vapor. The procedure followed in all these experiments was identical to that described in Chapter V for the tungsten surface. That is, the same instrumentation is used; the first step in the experimental procedure is to parallelize the emitter and collector surfaces; and finally the manner in which the variables are changed and the data recorded is also identical. For this reason the procedure will not be repeated here. Instead, the results obtained will be described and their correlation given.

1. RHENIUM BARE WORK FUNCTION

As pointed out above, the first step in the experimental program with this device was the determination of the bare work function of the rhenium surface. Two typical current-voltage characteristics used for this purpose are shown in Figures VI-1 and VI-2. In both cases a very well-defined saturation is evident. What is unusual in both of those curves and, as a matter of fact, is present in all such characteristics taken, is the very high reverse current. The reason for this current is that one of the cesium capsules, which was contained during outgassing in an appendage below the cesium reservoir, cracked sometime during this process. This resulted in the injection of a certain amount of cesium into the converter. Although

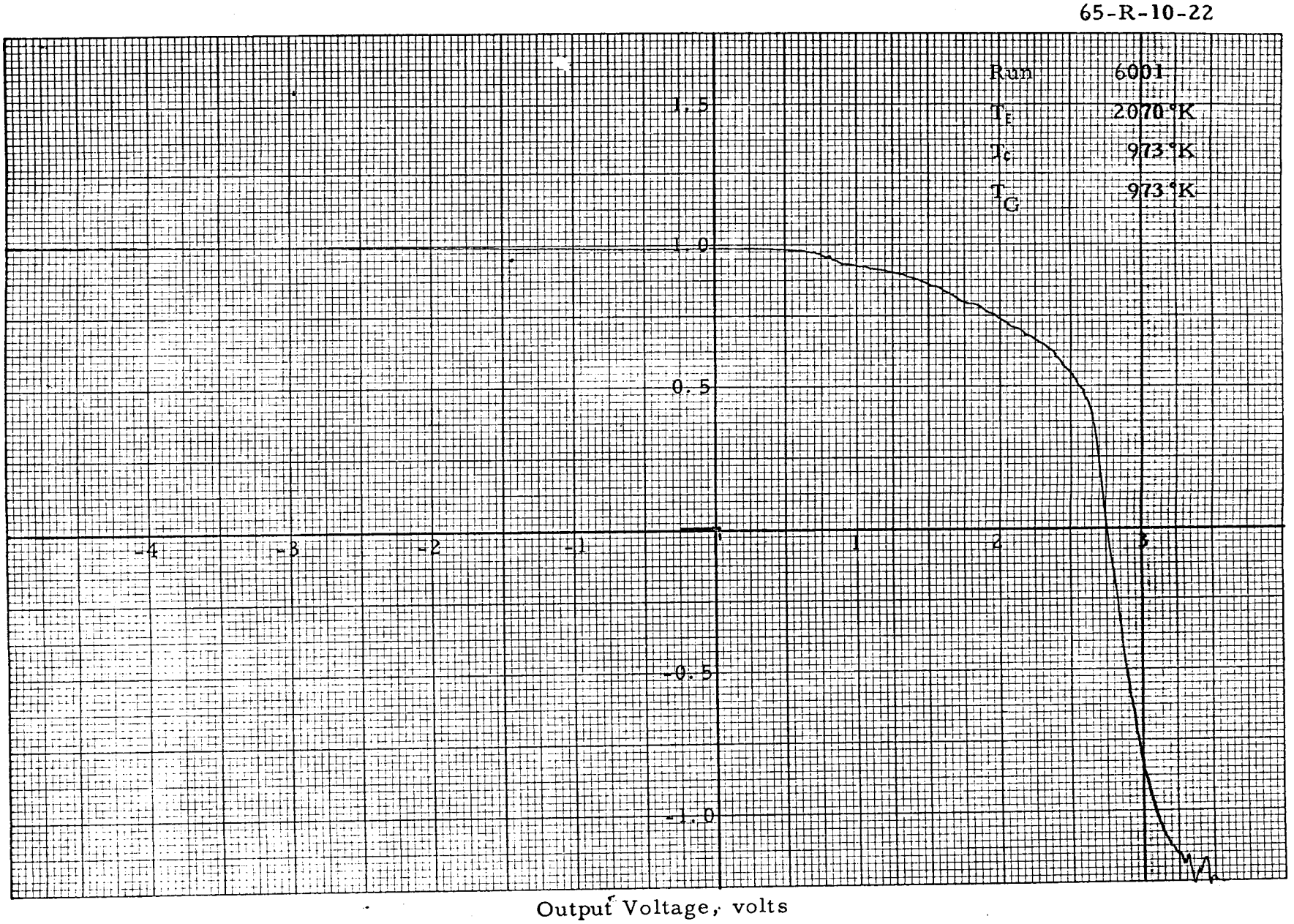

Figure VI-1. Typical J-V Characteristic used for "Bare" Work Function Determination.

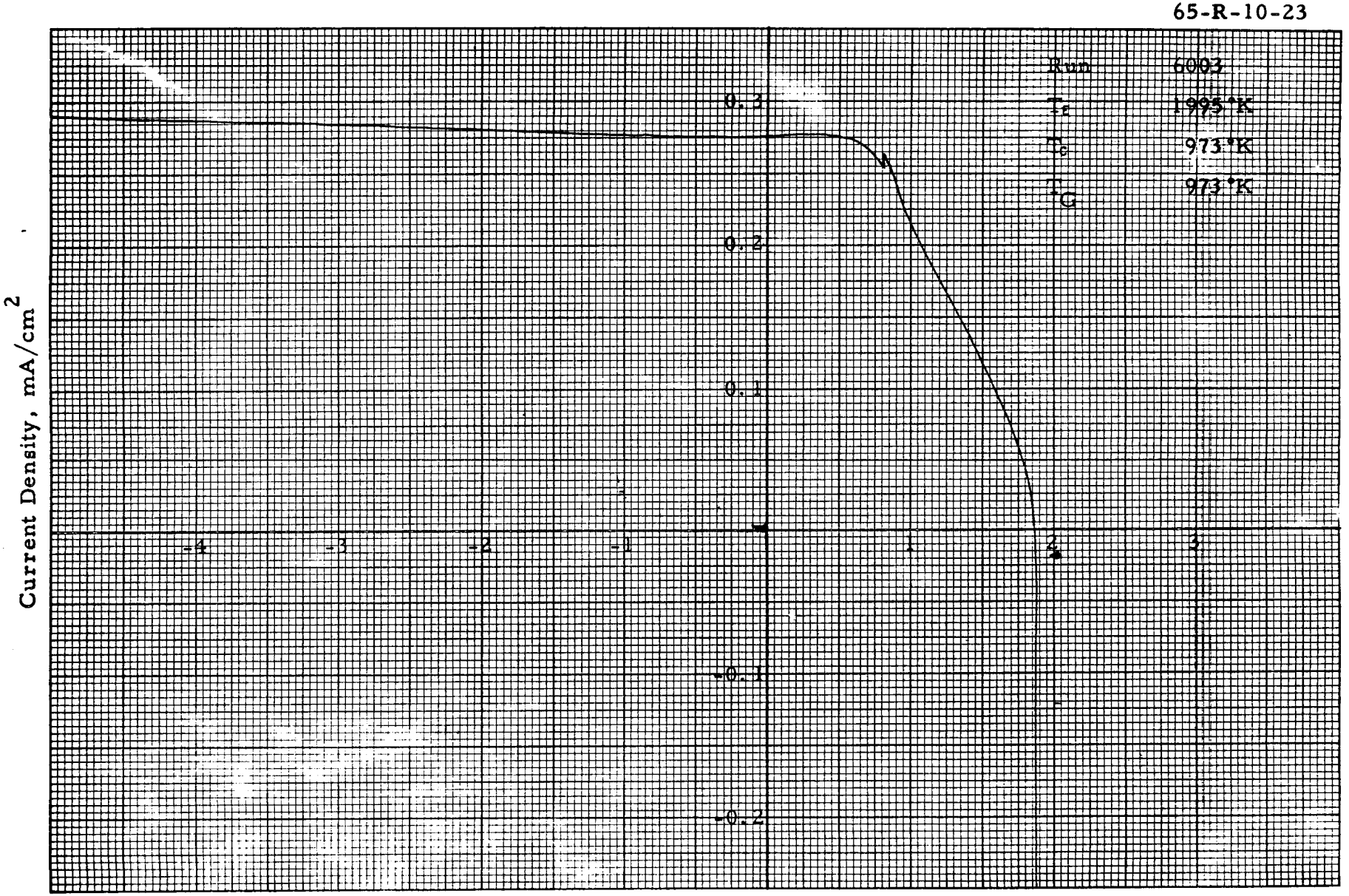

Figure VI-2. Typical J-V Characteristic used for "Bare" Work Function Determination.

insufficient cesium was present to lower the work function of the emitter surface, a fact which will be demonstrated later, nevertheless sufficient cesium was present to generate a very high ion current. This ion current is the one observed in these runs. To ascertain that the work function values obtained from these characteristics were, in fact, valid measurements, the results were plotted in the manner shown in Figure VI-3. This is a plot of saturation current versus the inverse emitter temperature, in which constant-work-function lines are shown. This plot is nothing more than a graphical presentation of the Richardson Equation. The points shown are the results of measurements described above, and at high temperatures they are seen to follow a constant-work-function line at 4.88 eV. At lower temperatures, higher $\frac{1}{T}$, the points deviate from a constant-work-function line and tend to give lower work function values. In that area, apparently, the temperature of the surface is low enough so that some cesium starts to adhere to it. The points above 2000°K emitter temperature are considered to be valid measurements of the bare work function of this surface.

2. CESIATED WORK FUNCTION

Figures VI-4 and VI-5 are typical characteristics used for determining the rhenium work function in the presence of cesium. Again, the well-defined saturation-current values from such plots are substituted in the Richardson Equation, along with the emitter temperature, and the Richardson work function value is obtained. With these measurements, however, a plot is made of work function versus the ratio of surface to reservoir temperature, rather than plots of the type shown in Figure VI-3. This plot is shown in Figure VI-6. Here the cesiated and bare work functions are plotted versus

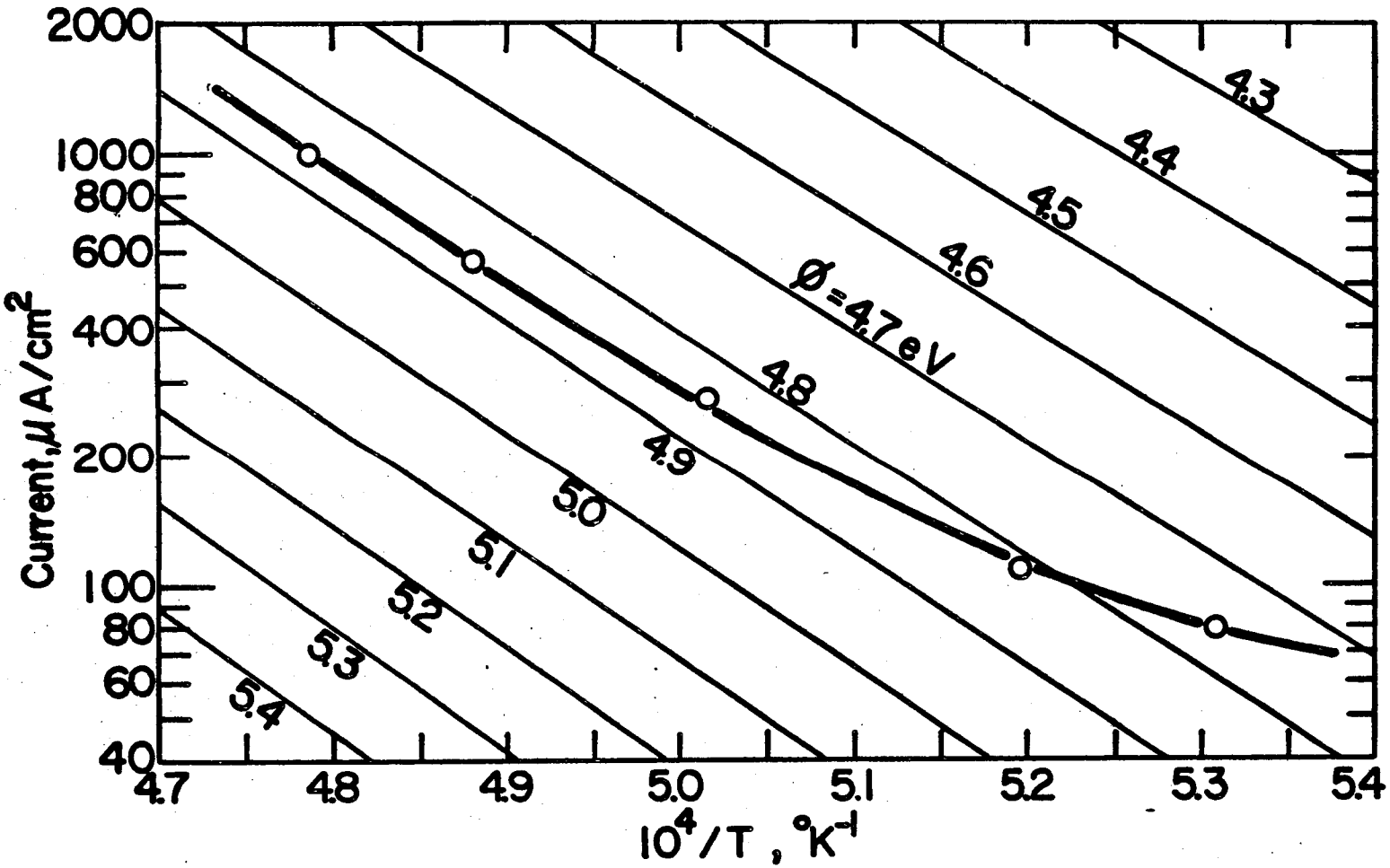

Figure VI-3. Plot of Richardson Equation.

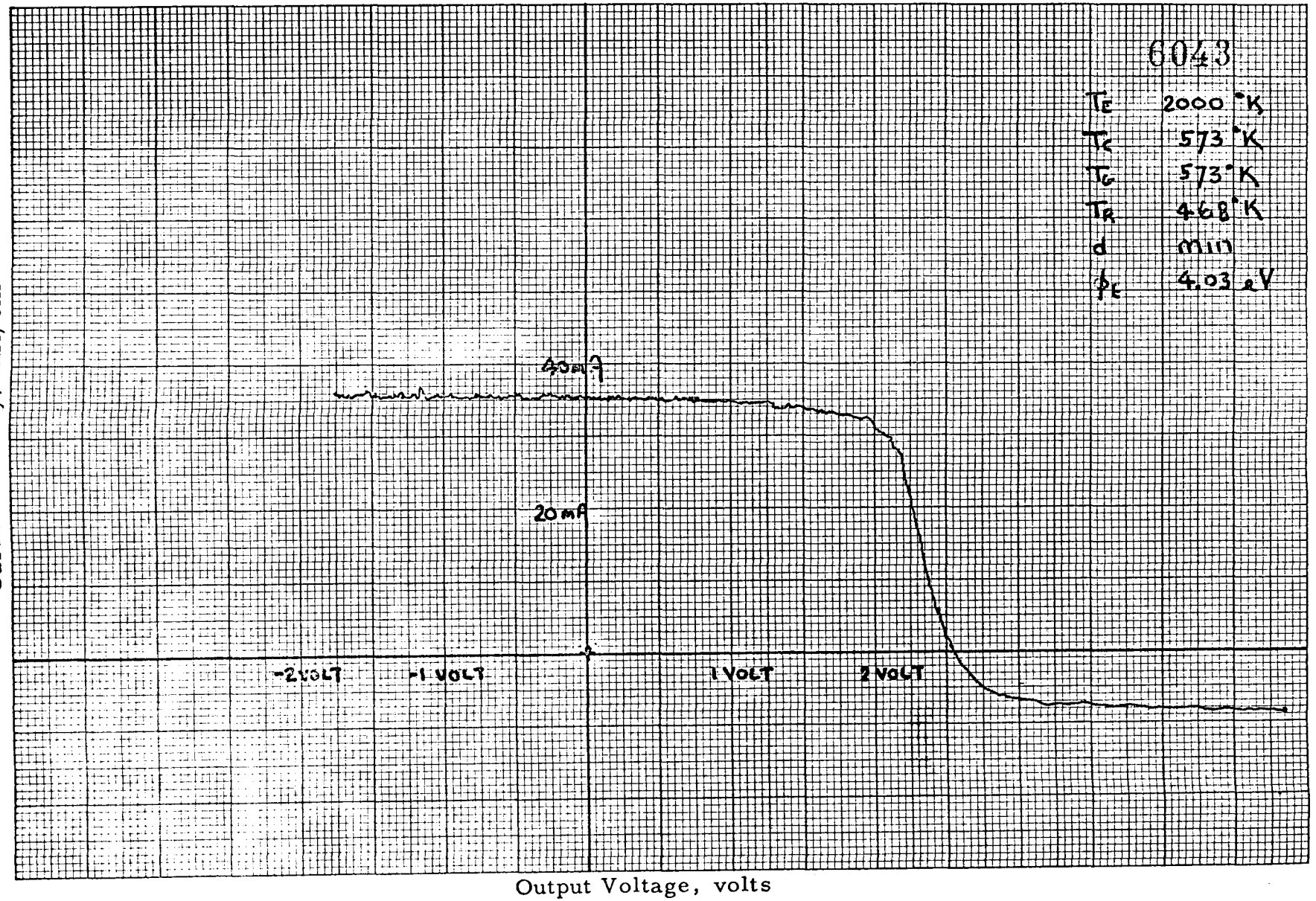

Figure VI-4. Typical J-V Characteristic used for Cesiated Work Function Determination.

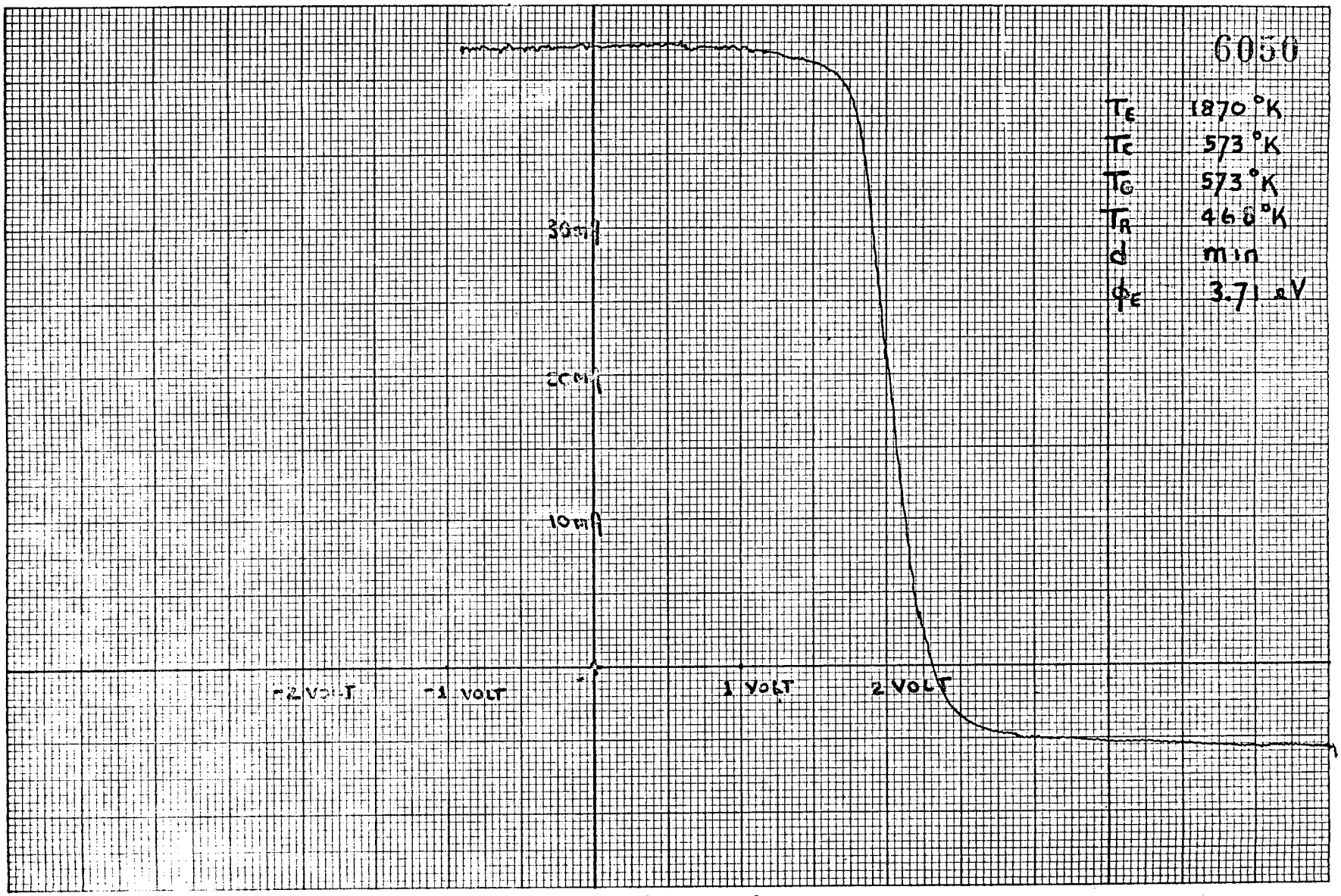

Figure VI-5. Typical J-V Characteristic used for Cesiated Work Function Determination.

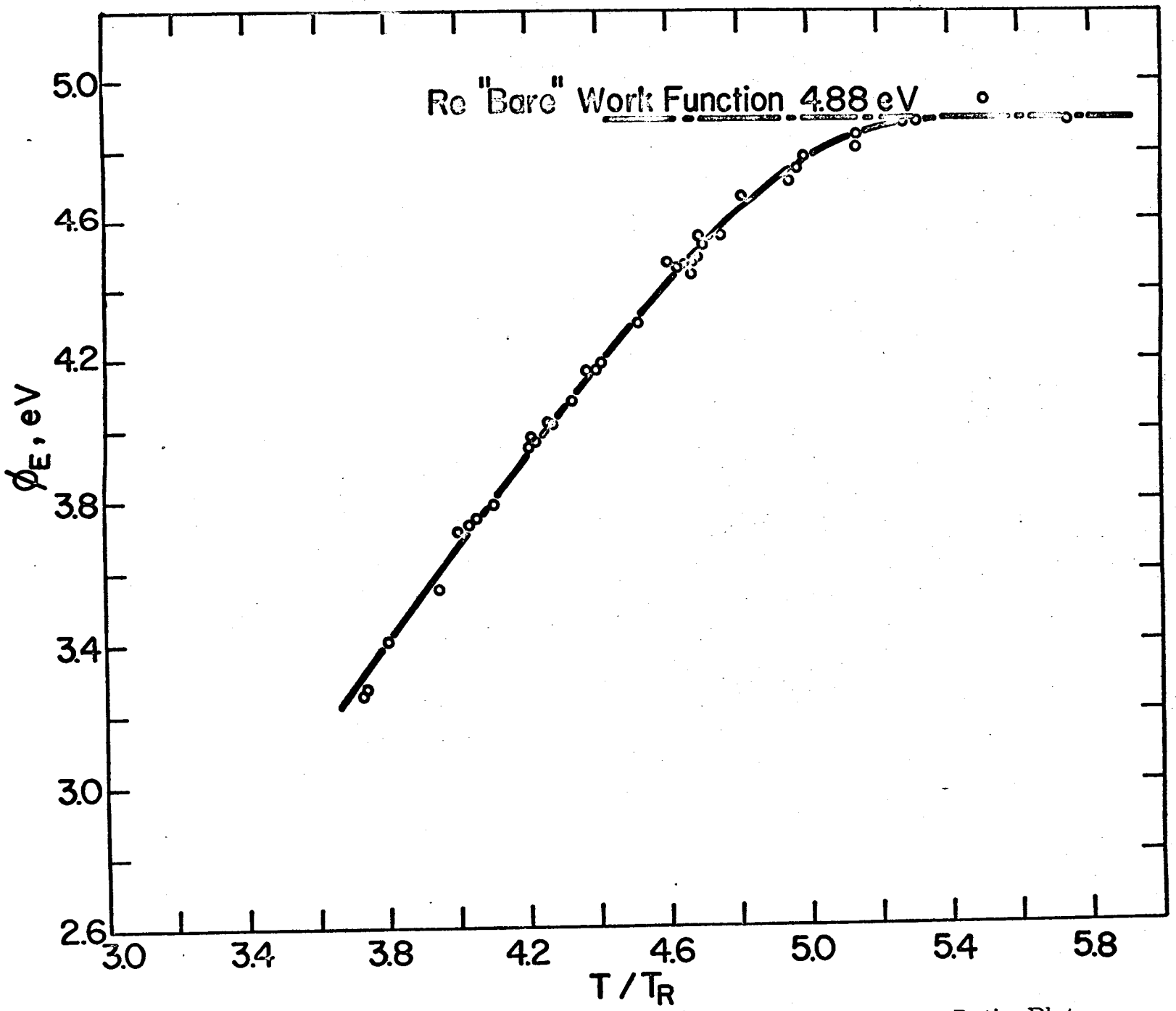

Figure VI-6. Work Function vs Surface-to-Reservoir-Temperature Ratio Plot of Cesiated Work Function Measurements.

the ratio of surface to reservoir temperature. The data obtained to date are identified as solid dots, and an asymptote labeled "Bare Work Function, 4.88", derived from the measurements mentioned above, is also indicated. The curve defined by these measurements in the presence of cesium approaches the bare-work-function asymptote smoothly. This, of course, was to be expected. The scatter in these data is surprisingly low. To compare the present results with the data obtained in the previous year, Reference 19, Figure VI-7 was prepared. This, again, is a plot of work function versus the ratio of surface to reservoir temperature. The present data are shown as a solid line together with the corresponding bare-work-function asymptote. The data of Reference 19 are shown as the dashed line, again with the corresponding asymptote. These two sets of data are probably the best illustration of the Rasor and Warner Theory obtained to date. Their bare-work-function asymptotes differ by about 130 mV, the bare work function for Reference 19 being 4.75 eV, and they behave very much as predicted by the theory in that they cross soon after a small amount of cesium coverage occurs at a T/T_R value of 4.7, the higher bare-work-function line falling lower than the other.

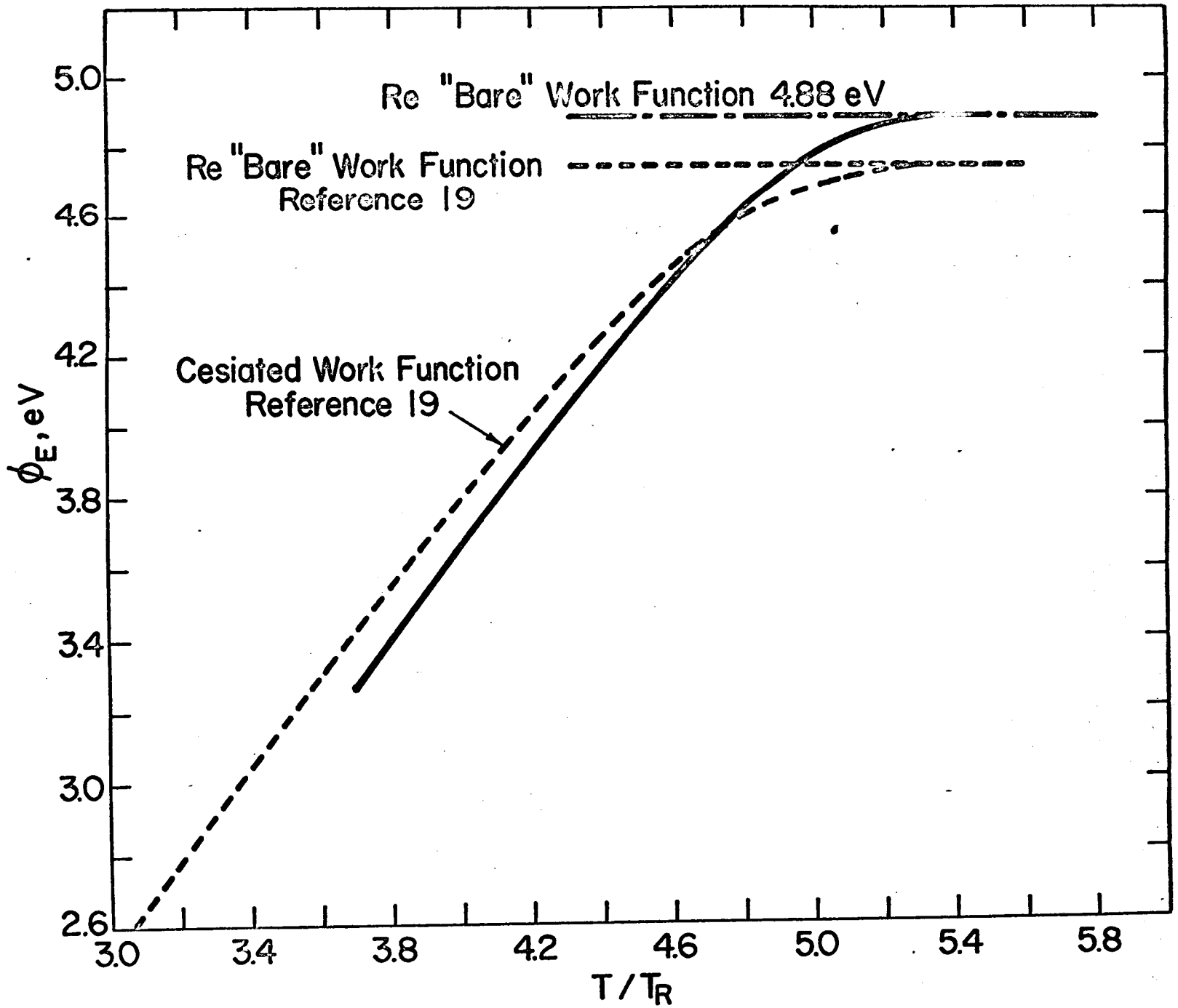

Figure VI-7. Comparison of Present Results with those of Reference 19.

CHAPTER VII

PLANS FOR NEXT QUARTER

In the course of the second quarter of the program, all three test vehicles will be operating almost continuously. The surface additive work will primarily consist of coverage studies on the emitter and collector. Initially these will be conducted with cesium fluoride only, and work function values will be mapped over wide ranges of variation of the emitter and additive reservoir temperatures. These, of course, were initiated in the first quarter of the program. In addition, time constants will be measured for the absorption and desorption of cesium fluoride as a function of surface temperature and cesium fluoride reservoir temperature, and, wherever possible, energies of activation for the absorption and the desorption process will be computed so that the time constants can then be predicted over the entire range of interest.

Once this phase is completed, cesium will be introduced to that test converter, and the work functions of the surface in the presence of both cesium and cesium fluoride will be measured again as a function of surface temperature, cesium fluoride reservoir temperature, and cesium reservoir temperature. Finally the time constants for these absorption and desorption processes will be measured near the end of the second quarter. No parametric work with this converter is planned for the second quarter.

The two converters intended for plasma additive experimentation will be charged with inert gas early in the second quarter, and the first step of the experimental program will consist of a documentation of any

effects of the inert gas on the work functions of the surfaces. Subsequent to that experiment, parametric work in the presence of the additive will be conducted, and, of course, one of the important variables will be the pressure of the inert gas. Specific experiments designed for the evaluation of any changes in the internal voltage drop of the converter as a result of the additive will be conducted.

The analytical work planned for the second quarter consists mainly of the computation of activation energies and their correlation with cesium fluoride coverage and pressure, and the effect of inert gas on the internal voltage drop. It is expected that correlations of the internal voltage drop similar to the ones obtained for the cesium-only case will be possible. It should be noted that no special problems or difficulties with the equipment or the experimental tasks have arisen up until this time, and therefore the schedule of the program is being followed quite closely.

REFERENCES

1. Ramsauer and Kollath, Ann. d. Physik 3, (1929) 536.

2. de Voto, Argon Plasma Transport Properties, Institute for Plasma Research, Stanford University, Report No. SUAA 217.

3. Powell and Brada, Proc. Roy. Soc. (London) A138, 117 (1932).

4. Chanin and Biondi, Phys. Rev. 107, 1219 (1957).

5. Brode, Phys. Rev. 34, 673 (1929).

6. Aberth et al, Atomic Collision Processes, N. Holland Publishing Co., p. 53.

7. Normand, Phys. Rev. 35, 1217 (1930).

8. Chen and Raether, Phys. Rev. 125, 2679 (1962).

9. Meyerand and Flavin, (Ref. 6, p. 59).

10. Bauer and Browne, (Ref. 6, p. 16).

11. Bruche, Ergeb. Exact. Naturwiss, 8, 185 (1929).

12. Massey, (Ref. 6, p. 3).

13. Jost and Kessler, Zeitchrift fur Physik 176, 126-142 (1963).

14. Warren and Parker, Phys. Rev. 128, 2661. (1962).

15. Caren, Phys. Rev. 131, 1904 (1963).

16. Brode, Phys. Rev. 5, 257 (1933).

17. Gould and Brown, Phys. Rev. 95, 897 (1954).

18. Brachmann and Fite, Phys. Rev. 112, 1157 (1958).

19. Kitrilakis et al, Final Report for the Thermionic Research Program, Task IV, Contract No. 950671, Report No. TE 7-66, prepared for Jet Propulasion Laboratory, Pasadena, California.